BRNO UNIVERSITY OF TECHNOLOGY

VYSOKÉ UČENÍ TECHNICKÉ V BRNĚ

CENTRAL EUROPEAN INSTITUTE OF TECHNOLOGY BUT

STŘEDOEVROPSKÝ TECHNOLOGICKÝ INSTITUT VUT

PATTERNING OF EXCITABLE CELLS ON MULTI-ELECTRODE ARRAYS

ZAROVNÁNÍ EXCITABILNÍCH BUNĚK NA MULTIELEKTRODOVÝCH POLÍCH

SHORT VERSION OF DOCTORAL THESIS

ZKRÁCENÁ VERZE DIZERTAČNÍ PRÁCE

AUTHOR — Ing. Jan Slavík

AUTOR PRÁCE

SUPERVISOR — doc. Ing. Jaromír Hubálek, Ph.D.

ŠKOLITEL

BRNO 2020

ABSTRACT

The work deals with the alignment of excitable cells on multielectrode arrays. First, the alignment of excitable cells was analyzed. Embryonic neurons from rat hippocampus and HL-1 cells, which are derived from the AT-1 line of tumor mouse atrial cardiomyocytes, were used. Alignment was tested on ridged surfaces and on surfaces with materials with different cellular affinities. It was demonstrated, that both neurons and HL-1 cells aligned in direction of ridges on ridges surface, but only neurons aligned on surface with different chemical affinity. Further, own multielectrode arrays were made, the HL-1 cells were cultured on the multielectrode arrays, and the action potentials of the HL-1 cells were measured and analyzed. The aim was to prove that it is possible to measure the action potential on the fabricated multi-electrode arrays. A special multielectrode array with a uniform surface was made to align cells on a multielectrode array. This multielectrode array is called a planar multielectrode array. The planar multielectrode arrays were made by a special fabrication process. The layers of the planar multielectrode array were deposited on the sacrificial substrate in the reverse order. The sacrificial substrate for deposition was silicon wafer on which was deposited another sacrificial layer from gold. The upper insulating layer of planar multielectrode array was deposited first and the lowest substrate layer was deposited last. Then the planar multielectrode array with the sacrificial gold layer was peeled off from silicon due to the low adhesion of gold to silicon and planar multielectrode array turned upside down. The sacrificial gold layer was removed by a wet etchant and planar multielectrode array was finished. On a planar multielectrode array, the HL-1 cells were patterned into strips by a chemical method using a combination of microprinting of an adhesive agent and subsequent coating by an anti-adhesive agent of not microprinted areas. The electrophysiological properties of aligned HL-1 cells were measured using the planar multielectrode array. By this experiment, it was introduced fabrication technology for fabrication of planar multielectrode arrays and the planar multielectrode array was successfully tested for HL-1 cells alignment on its surface by combination of microprinting of an adhesive agent and anti-adhesive agent coating.

KEYWORDS

neurons, HL-1 cells, cells alignment, multielectrode array, microprinting, adhesive, anti-adhesive

ABSTRAKT

Práce se zabývá zarovnáváním excitabilních buněk na multielektrodových polích. Nejprve bylo analyzováno zarovnávání excitabilních buněk. Byly použity embryonální neurony z hippocampusu potkanů a HL-1 buňky, které jsou odvozeny z AT-1 linie nádorových myších atriálních kardiomyocytů. Zarovnávání bylo testováno na drážkovaných površích a na površích s materiály s různou buněčnou afinitou. Bylo prokázáno, že na drážkových površích se ve směru drážek zarovnávají neurony i HL-1 buňky, ale na površích s různou chemickou affinitou se zarovnávají pouze neurony. Dále byly vyrobeny vlastní multielektrodová pole, na těchto multielektrodových polích byly kultivovány HL-1 buňky a byl změřen a analyzován akčních potenciál HL-1 buněk. Cílem bylo prokázat, že je možné měřit akční potenciál na vyrobených multielektrodových polích. Pro zarovnání buněk na multielektrodovém poli bylo vyrobeno speciální multieletrodové pole s uniformním povrchem. Toto multielektrodové pole je nazýváno planární multielektrodové pole. Planární multielektrodové pole bylo vyrobeno speciálním vyrobním procesem. Vrstvy planárního multielektrodového pole byly deponovány na pomocný substrát v opačném pořadí. Pomocný substrátem pro depozici byla křemíková deska, na který byla nadeponována další pomocná vrstva zlata. Horní izolační vrstva planárního multielektrodové pole byla deponována jako první a nejspodnější vrstva substrátu byla nadeponována jako poslední. Planární multielektrodové pole i s pomocnou zlatou vrstvou bylo strhnuto s křemíku díky nízké adhezi zlata ke křemíku a planární multielektrodové pole se otočilo vzhůru nohama. Pomocná zlatá vrstva byla odstraněna mokrým leptadlem a tím bylo planární multielektrodové pole dokončeno. Na planárním multielektrodovém poli byly zarovnány HL-1 buňky do pruhů chemickou metodou pomocí kombinace otisku adhezní látky a následným potažení neotisklých ploch anti-adhezní látkou. Elektrofyziologické vlastnosti zarovnaných HL-1 buněk byly změřeny pomocí planárního multielektrodového pole. Tímto experimentem byla představena výrobní technologie pro výrobu planárních multielektrodových polí a toto planární multielektrodové pole bylo úspěšně testováno pro zarovnání HL-1 buněk na jeho povrchu kombinací otisku adhezní látky a potahování antiadhezivním činidlem.

KLÍČOVÁ SLOVA

neurony, HL-1 buňky, buněčné zarovnávání, multielektrodové pole, razítková metoda, adhezní, antiadhezní

SLAVÍK, J. *Patterning of excitable cells multi-electrode arrays*. Brno: Brno University of Technology, Central European Institute of Technology, 2020. 40 p. Thesis supervisor doc. Ing. Jaromír Hubálek, Ph.D.

DECLARATION

I certify that the work presented in this thesis was performed independently, under the supervision of doc. Ing. Jaromír Hubálek, Ph.D., and is original with the sole exception of the technical literature and other sources of information that are acknowledged in the text and reference list, and that the material has not been submitted, in whole or in part, for a degree at this or any other university.

Brno . . . . . .

. . . . . .
(author's signature)

ACKNOWLEDGMENT

I would like to thank doc. Ing. Jaromír Hubálek, Ph.D. for supervision and support during my work on dissertation.
CzechNanoLab project LM2018110 funded by MEYS CR is gratefully acknowledged for the financial support of the measurements/sample fabrication at CEITEC Nano Research Infrastructure.

Brno . . . . . .

. . . . . .
(author's signature)

Table of contents

1. Introduction

Electrical signals are one of the ways of signal transmission for communication between cells of eukaryotic organisms. In the human body, electrical signals are used primarily for muscle contraction, including heart contraction, and for signal transmission between neurons or between neurons and other cells.

It have been developed methods to study electrophysiology *in vivo* and *in vitro* at various levels of biological systems, from individual ion channels on the plasma membrane to the study electrophysiology of whole tissues. Multi-electrode array (MEA; also known as a microelectrode array) represent one of these levels to study electrophysiology at the level of cell populations.

The MEA is used to study dynamics of electrical signal transduction of neural and hearth cells populations or tissues. MEAs can be applied *in vivo* and *in vitro*. MEAs for *in vitro* are applied on cells or tissue slices, which are cultured on the surface of the MEA. The MEA measures extracellular signals from cells, cells are not damaged by measurement and that allows long-term measurements. MEAs are applied to the study of electrophysiology, cell-based biosensors, drug discovery and pharmacology.

Some cells in the bodies of organisms are organized in aligned directions. This cell alignment affects the physiology of individual cells and whole tissue function. The induction of conditions for cell alignment *in vitro* makes it possible to preserve or mimic certain properties which correspond to properties of the cells *in vivo*. Alignment of excitable cells is essential for the function of nervous and cardiac tissues. Cells adhering to the flat bottom of the culture flask may lose their morphology, whereas cells adhering to special substrates may retain or mimic the morphology *in vivo*. The alignment of cells on MEA has limitations because the MEA, as the substrate for cells cultivation, cannot be arbitrary. The insulation layer and the electrodes, which are essentially the substrate for cell cultivation, must be made from materials with suitable electrical properties. Therefore, one of the directions of MEA development is focuses on MEA for cells alignment and patterning.

This work focuses on the possibilities of patterning neuronal cells and cardiac cells and the production of MEA with a completely planar surface suitable for cell patterning using the micro-stamp method.

2. State of art

2.1. Excitable cells

2.1.1. Membrane potential and action potential

Excitable cells are specialised cells in multi-cellular organisms. Excitable cells can be stimulated resulting in generation of an action potential. Excitable cells in human bodies include neurons, cardiac muscle cells, skeletal muscle cells, smooth muscle cells and some types of endocrine cells. [1, 2]

All living cells have a cell membrane which separates the intracellular space of the cell from the extracellular environment. The cell membrane maintains different concentrations of ions in the extracellular and intracellular spaces; this causes different voltages on inner and outer sides of the cell membrane and this voltage difference is called the membrane potential. [1-7]

All living cells have membrane potentials; however, only the excitable cells can change their membrane potentials and bring about the action potential. The action potential can be defined as a local rapid rise and fall of the membrane potential. The action potential is caused by opening ionic channels on the cell membrane and thus changing ions concentrations and thus changing of membrane potential. The action potential is one way of fast transfer of signals between cells and on the cells. [2, 7]

2.1.2. Structure on neurons

The neurons are highly specialised cells for cell-to-cell communication by synapse. The function of neurons divides them into sensory neurons, motor neurons and interneurons. Neuron bodies, axons and dendrites are the most common parts of neurons. The neuron body draws on an inner chemical pathway to receive signals from dendrites and send signals to axons. The axons are long, slender projections of neurons which send signals from the neuron body to the synapse by the action potential. The action potential propagate on axon membrane to the end of the axon where the synapse is located. At the synapse, the signal is passed from cell to cell electrically or chemically. In the case of neuron-to-neuron communication, the signal is usually received by the dendrite and the dendrite transfers the signal through the chemical pathway to the neuron body where the signal is further processed. [1, 2, 7]

2.1.3. Structure of pacemaker cells and cardiomyocytes

The heart is a muscular organ with two types of muscle cells: pacemaker cells and cardiac muscle cells (cardiomyocytes). The function of the pacemaker cells is to initiate and distribute the action potential over the heart and the function of cardiomyocytes is to ensure synchronised and regular beat rates of the heart.

The pacemaker cells induce the spontaneous generation of the action potential. The pacemaker cells are organised into fibres, which transfer the action potential to the cardiomyocytes [1, 2, 5]. Cardiomyocytes form the muscular walls of the heart chambers. The spreading of the action potential to the cardiomyocytes is accompanied by their contraction, and so, the contraction of the whole heart. The cell contraction is caused by specialized organelles called myofibrils which consists of units known as the sarcomeres. Both the pacemaker cells and cardiomyocytes are capable of contraction. However, the pacemaker cells have a disorganised sarcomere structure, and so, pacemaker cells are not effective for contraction [8].

Action potential spreads over the cardiac cell membrane, but signal between cardiac cells is transferred by changing inner ions concentration through structure known as the intercalated disc, which connect cardiac cells. [2–6, 9]

The pacemaker cells are organised into fibres, but the cardiomyocytes create a continuous layer. The individual cardiomyocytes have a longitude shape. The longitudinal shape of the cardiomyocytes is important for the coordinated contraction of the heart; it also affects the transfer of the action potential from one cell to another. The velocity of the action potential transfer is approximately 50 $cm \cdot s^{-1}$ [10]. The ratio of longitudinal conduction velocity to transverse conduction velocity is approximately 2:1. This difference is caused by cardiomyocytes' longitudinal shape and the high amount of connexins at the end of the short sides of cardiomyocytes [11]. In the human body, cardiomyocytes have a cylindrical shape, with a length of about 60–140 μm and a width of 17–25 μm [12]. The cardiomyocytes' shape is important for proper heart contraction.

2.2. Methods for cell alignment *in vitro*

Cell alignment plays an important role in the proper functioning of some cell types. Aligned cells necessary for cell organisation are located in the muscle and the nerve tissue; these aligned cells are important for biomechanics, cell biology, tissue engineering and regenerative medicine applications. Under common *in vitro* conditions, the cells are not aligned, but cell alignment can be induced by various approaches. Methods for cell alignment are often bioinspired. These methods try to replicate *in vivo* conditions to induce cell alignment, as well as to induce a variety of other cell functions including morphology, growth, proliferation, inner cell reorganisation, adhesion, contraction, activation of intracellular and extracellular pathways and gene expression. The most common methods for cells alignment are chemical surface treatment and topographical patterning: [13]

Chemical surface treatment – between the cell that adheres on a surface and the surface itself is an interlayer of proteins. In short, cells do not adhere directly on the surface of the substrate, but rather on the proteins (and extracellular matrix). Accordingly, cell adhesion depends primarily on surface properties to promote or prevent protein adsorption. The whole surface of the culture flask is coated by an adhesion-promoting agent to support cell adhesion. However, the coating of the coating agent can be selectively patterned, and the cell will align according to the pattern. The most common approach to pattern coating agent is called microprinting, also known as soft lithography. The principle behind microprinting is the fabrication of soft, flexible polydimethylsiloxane (PDMS) with elevated features (referred to as the stamp). The PDMS stamp will be coated by the coating agent, washed, dried and pushed against the substrate for cell cultivation. The coating agent will be printed only from the elevated features of the PDMS stamp and thus, cells will adhere on printed coating agent. [13, 14]

Topographical patterning – some cells *in vivo* live inside an extracellular matrix network, and the extracellular matrix forms cues according to which cells are aligned. The approach to cell alignment is the fabrication of structures, the dimensions of which replicate the surface on which cells grow *in vivo*. The most common of these structures are 3D scaffolds, ridges, pillars, pits and surface roughness (names of structures can vary). These structures can be made to selectively create patterns, while the ridges are only structures with an orientation (isotropy). The effect of topographies on cell alignment could vary for different cell types and surface topographies. [13, 15]

2.3. Concept of MEA for application *in vitro*

A MEA is a term used for devices consisting of an array of insulated microelectrodes that measure the action potential of cell populations. The MEA for application *in vitro* usually consists of a glass substrate, an array of tens to hundreds of insulated electrodes at dimensions from tens to hundreds of micrometres, a much bigger reference electrode and a glass ring glued via PDMS onto MEA to create reservoir for cell cultivation. Dissociated cells or tissue slides can be cultivated on the MEA. The scheme of MEA is shown in Figure 1. Dissociated cells are cultivated directly on the electrodes, which measure extracellular field potentials generated by the action potential of the excitable cells. The MEA can measure the action potential simultaneously from all electrodes; moreover, the MEA can stimulate cells via voltage or current impulses. The MEA electrodes can be organised as a two-electrode or three-electrode system. For the three-electrode system, the action potential is measured by a working electrode. Measured potential is between working electrode and reference electrode and current flows from working electrode through

the cultivation medium (electrolyte) to counter electrode to close the circuit. For the two-electrode system, the counter electrode serves also as the reference electrode. Both two- and three-electrode systems are used for MEA. A MEA has from tens to hundreds of working electrodes, but usually only one counter electrode and one reference electrode. The measured signal is 100-1000x amplified by a two-stage low-noise amplifier and then filtered. The entire measuring system to measure cells action potentials consists firstly of the MEA itself; the MEA pads are contacted by a headstage with preamplifiers, which is connected to an interface board that is itself connected to a computer with a software interface. Between the optional parts of the measuring system is the heater of the MEA and the camera. The MEA provides non-invasive, long-term measurements to study the electrophysiology of cell populations in cardiology and neuroscience. [16, 17]

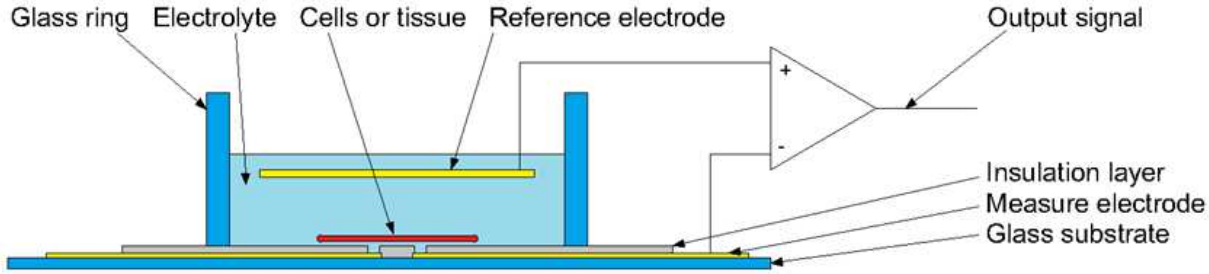

Figure 1: The MEA scheme.

3. Aim of Thesis

The aim of this work is to propose technology for MEA, and demonstrate procedure for excitable cells patterning on MEA. The work is divided into the following partial aims, which have their own chapters:

Fabrication of substrates for neurons patterning. Ridges on quartz bulk substrates is considered as topographical structures and parylene structures on quartz substrate are materials with different chemical affinity and it is consider as chemical surface treatment. Develop algorithm for neurons alignment analysis. Analyse neurons patterning by topographical structures and chemical surface treatment.

Fabrication of substrates for HL-1 cells (cardiac-like cells) patterning. Ridges on various bulk substrates is considered as topographical structures and parylene structures on glass substrate is consider as chemical surface treatment. Develop algorithm for HL-1 cells alignment analysis. Preparation of various substrates for HL-1 cells proliferation analysis. Analyse HL-1 cells proliferation and patterning by topographical structures and chemical surface treatment.

Optimize fabrication technology for standard MEA, cultivate HL-1 cells on MEA and measure HL-1 cells action potential.

Develop and optimize fabrication technology for MEA with fully planar surface. Patterning HL-1 cells on planar MEA surface by microprinting method with combination of anti-fouling agent coating. Measurement of electrical properties of patterned HL-1 cells.

4. Hippocampal neurons patterning on quartz and parylene ridges

Partial results of the presented work in this chapter have been submitted in [18].

4.1. Introduction

Neurons are cells with a specific morphology characterised by long axons and dendrites. During their growth in a developing brain, neurons are precisely patterned by signalling and the physical topography of the environment. The topography of the environment forms radial glial cells in shape of ridges, which together create scaffolds. These scaffolds serve as pathways for the migration of neurons [19-25]. Neurons patterning is a complex mechanism, and approaches for directional neuron growth have thus been investigated both *in vivo* and *in vitro* [26-28]. To reveal only the isolated effect of neuron patterning by topography, neuron alignment is researched *in vitro*. Similar to *in vivo* surface topography, tested artificial topography includes ridges. Longitudinal alignment on parallel ridges has been observed in several studies [29-32]. Although most neurons align longitudinally with the direction of the ridges, in certain conditions, some neuron types cultivated on parallel ridges can align longitudinally or transversally [33-35]. These experiments show that neurons can react differently on ridges with different dimensions and that neurons alignment is an active rather than passive process.

The aim of this chapter is to describe difference of neurons alignment on quartz ridges structures for topographical patterning and parylene ridges on quartz substrate for chemical patterning. The aim is also to elaborate effect of neurons alignment on different substrates, with emphasis on different dimensions of the substrate rather that studying the subtle dimensional differences.

4.2 Materials and methods

4.2.1. Substrate fabrication

Substrates for neurons patterning were fabricated by microfabrication methods. Briefly, substrates were 2 inch quartz wafers and 2 inch quartz wafers with thin layer of parylene C. Substrates were coated by photoresist, structure design was exposure by through a photolithographic mask and photoresist was developed. Then structures were etched by reactive ion etching (RIE) and photoresist was removed. All samples were cleaned by oxygen plasma.

Four types of test substrates were fabricated: quartz substrate with ridges 0.25 µm high, quartz substrate with ridges 1 µm high, quartz substrate with ridges 4 µm high, and parylene ridges 0.25 µm high etched on the quartz substrate. The structures for each substrate have the same design: namely, blocks of 2 µm-wide lines, 4 µm-wide lines, 6 µm-wide lines and 8 µm-wide lines. The distances among lines were the same as the lines' width. The design also contains structures with various shapes to facilitate the qualitative study of the neurons' adhesion. The scheme of the fabricated substrates is shown in Figure 2.

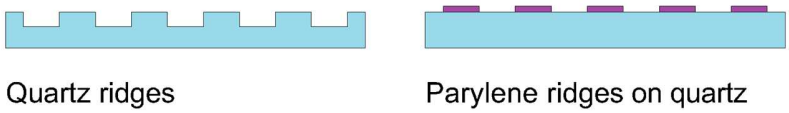

Figure 2. Scheme of quartz ridges in bulk quartz substrate and parylene ridges on quartz substrate.

4.2.2. Neurons isolation, seeding, cultivation, immunostaining and visualisation

Neurons used for experiments were hippocampal neurons isolated from brains dissected from Sprague Dawley rat pups at the 18th day of pregnancy. Neurons isolation, cultivation and immunostaining staining was performed on the basis of published protocol [36]. Test substrates were coated by poly-D-lysine, neurons were seeded at a concentration of 2000 neurons per cm^2 and neurons immunostaining was done after 7 days of neurons cultivation on test substrates. Samples were observed by fluorescence microscope.

4.2.3. Image and data analysis

To analyse the neuron alignment, a tracing algorithm was created in the scripting programming language of the MATLAB programming environment. The input is a fluorescence image of neurons. Neurons are transformed into the neurons' skeletons, pixels are demarcated at places of neuron connection and furcation, and thus, neurons are separated into the individual line segments. From the identified line segments, line lengths and angles from 0° – 90° are calculated (0° is horizontal plane, 90° is direction of ridges); from all other directions, the angle can be mirrored into the range 0° – 90°.

For each substrate and its ridge blocks, line segments were divided into angle groups of 5° (i.e. 0° - 5°, 5° - 10°, ..., 85° - 90°, for 18 angle groups in total), after which the lengths of each line segment were summed within the angle group. For each substrate and its ridge blocks, the angle of the lowest directional neurons' growth from the angle group distribution was calculated. The equation for the lowest directional neuron growth is as follows:

$$Angle_{min} = \frac{\sum_{i=m}^{n}\left(A_i \frac{N_m}{N_i}\right)}{M} \quad (1)$$

where $Angle_{min}$ denotes the angle of the lowest directional neuron growth (°), n is the angle group with the highest length until the angle group 0-5° is reached, m is the angle group with the lowest length, A_i is the middle angle from the angle group (e.g., for the angle group 10-15°, it is 12.5°), N_m is the lowest length of angle group m (µm), N_i is the length of angle group n (µm) and M is the number of calculated angle groups (-).

The neuron alignment was evaluated in the form of two ratios. The first ratio was calculated as follows:

$$Align_{abs} = \left(\frac{angle\_group_{85-90}}{angle\_group_{0-85}}\right) \quad (2)$$

where $Align_{abs}$ is the absolute neuron alignment (-), $angle\_group_{85\text{-}90}$ is the length of the angle group 85° - 90° and $angle\_group_{0\text{-}85}$ is the summed length of the angle groups from 0° – 5° to 80° – 85°.

The second ratio was calculated as follows:

$$Align_{rel} = \left(\frac{angle\_group_{45-90}}{angle\_group_{0-45}}\right) \quad (3)$$

where $Align_{rel}$ is the relative neuron alignment (-), $angle\_group_{45\text{-}90}$ is the summed length of the angle groups from 45° - 50° to 85° - 90° and $angle\_group_{0\text{-}45}$ is the summed length of the angle groups from 0° – 5° to 40° – 45°.

4.3. Results and discussion

Examples of neurons adhesion and alignment on quartz and parylene structures and ridges is shown in Figure 3. The distribution of the neurons' directional growth for each ridge block from each substrate is shown in Figure 4. The absolute alignment equation (2) evaluate how tightly neurons follow the individual ridges and results is shown in Figure 5. And the relative alignment equation (3) evaluate overall tendency of the neurons to grow in the longitudinal direction of the ridges and results is shown in Figure 6.

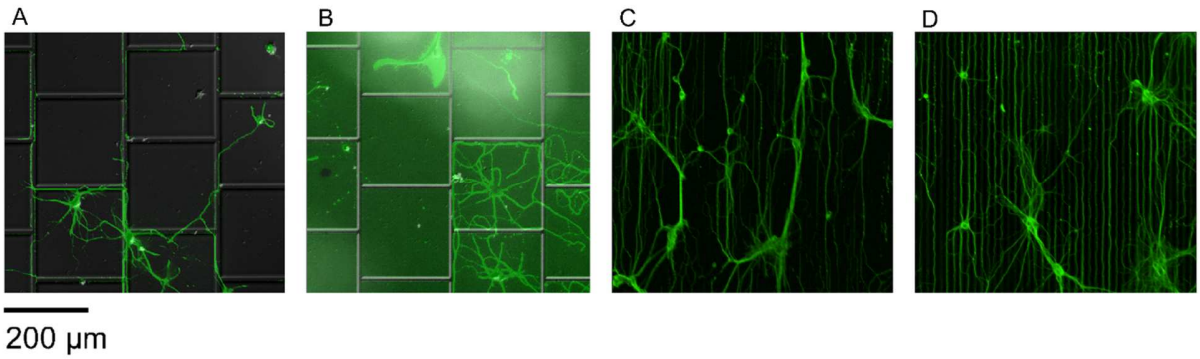

Figure 3: The growth of neurons on test structures. A: Quartz squares of 150 µm separated by grooves 8 µm wide and 4 µm high. B: Parylene squares of 150 µm separated by grooves 8 µm wide. C: Quartz ridges 8 µm wide and 4 µm high. D: Parylene ridges 8 µm wide.

Neurons on quartz structures have a tendency to adhere to the bottom and stick to structures walls. For quartz ridges, the most effective neuron alignment is for high ridges, while the effectivity of ridge width varies according to the ridges' height. For small ridges, smaller width is better, while for high ridges, a larger width is better. This is probably cause by too deep and too narrow space, where neurons cannot fit to follow the wall of the ridge. For parylene structures, neurons have a tendency to adhere on parylene rather than quartz, so neurons grows preferably on parylene and thus for parylene ridges (long and thin structures), neurons follows direction of parylene ridges.

For absolute alignment, parylene ridges are more effective than quartz ridges, however for relative alignment difference is not so high, even some quartz ridges are almost same effective for neurons alignment as parylene ridges. This show that neurons have overall tendency to grow in the longitudinal direction of quartz ridges, even if the neurons are not stuck to the ridges' walls, however on parylene ridges, neurons have tendency to follow individual parylene ridges.

If it is considered that neurons should align in longitude direction of ridges (that is angle 90°), then the lowest direction of neurons should be in angle 0° (2.5° as middle angle from the angle group with lowest length). However from the distribution of neuron growth direction shows that the lowest angle of neurons direction alignment is from 8.08° to 19.13° for tested substrates. For quartz ridges, it can be explained by two phenomena. Firstly, one neuron try to connect with other neuron in the shortest direction, what can

be transversal direction for longitude neurons alignment direction or secondly, neurons sensing their surroundings and thus crossing the ridges in transversal direction as small tendency for transversal alignment. And for parylene ridges, neurons which do not follow parylene ridges have tendency to cross to another parylene ridge or another neuron in the shortest direction, what is also transversal direction.

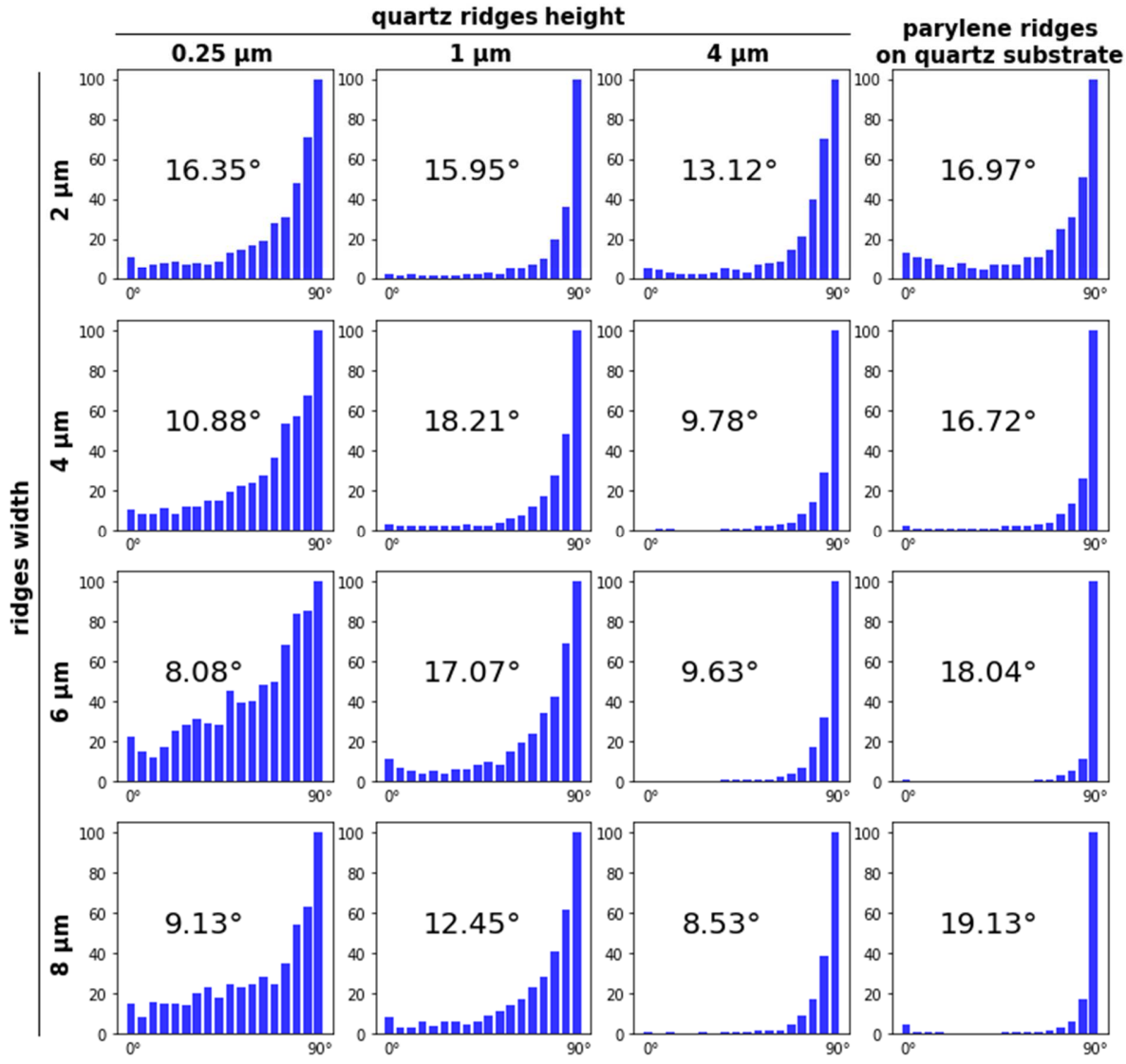

Figure 4: The distribution of neuron growth direction. Numbers in graphs are the angles of the lowest directional neuron growth.

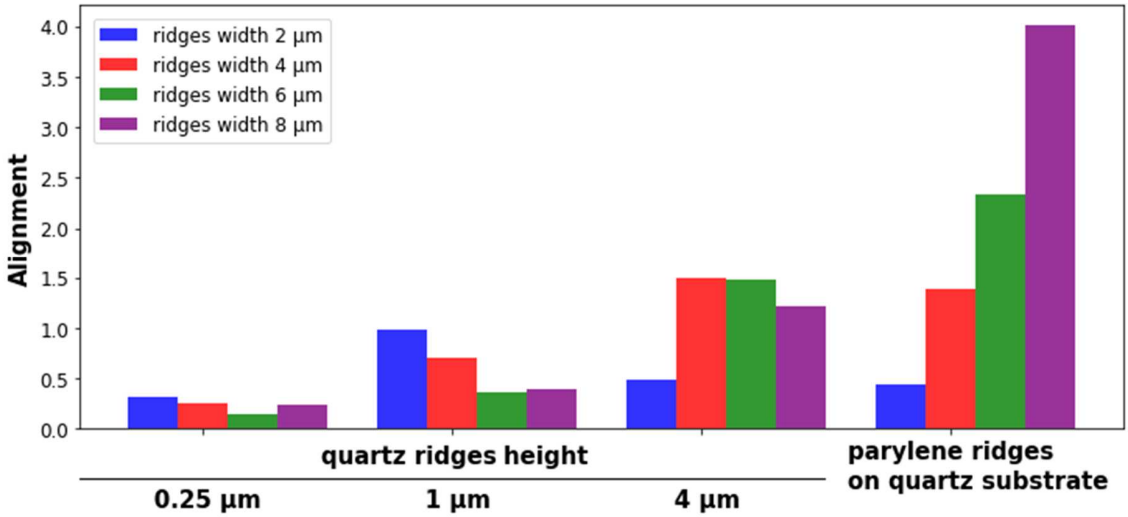

Figure 5: The absolute neuron alignment.

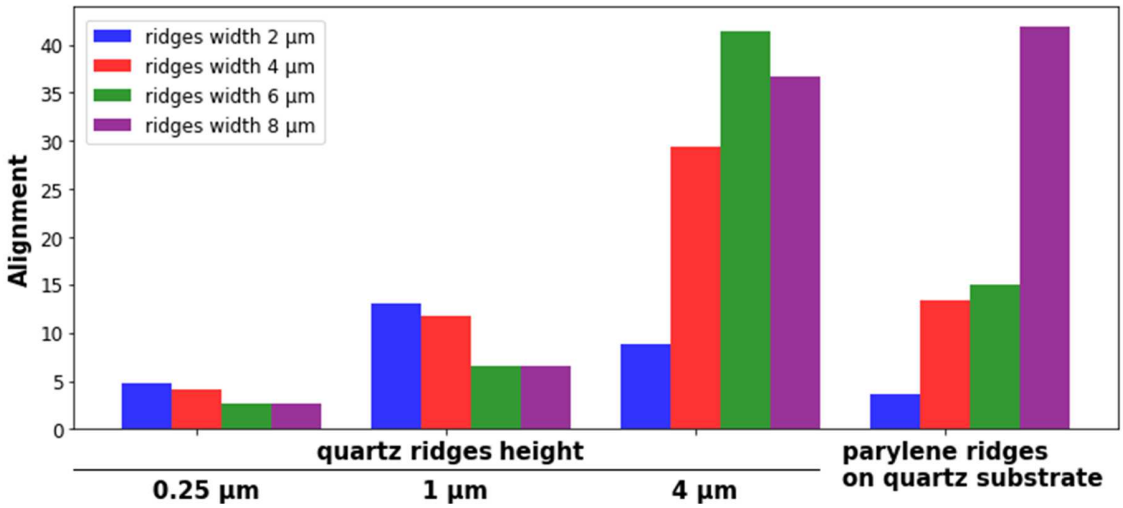

Figure 6: The relative neuron alignment.

5. HL-1 cell alignment and proliferation on silicon, silicon dioxide, PDMS and parylene ridges

5.1. Introduction

How was already mentioned, a human cardiomyocyte has a cylindrical shape, with length of around 60-140 µm and width 17-25 µm [12]. The cardiomyocytes' morphology supports both their function and the overall organisation of the cardiomyocytes in the heart tissue. Cardiomyocytes' differentiation and alignment are facilitated by a scaffold on which they grow. The scaffold is formed from an extracellular matrix of fibroblasts and the cardiomyocytes itself. [37]. Isolated cardiomyocytes lose their morphology during cultivation. While some cardiomyocytes can retain their cylindrical shape, most of them change

their shape to oval shape or round shape. The loss of cylindrical shape morphology is accompanied by a loss of myofibrils, and thus lower contractility and a non-uniform contraction rate. [38] Inducing cardiomyocyte alignment allows for the study of more representative cardiomyocytes *in vitro*; it also has other applications, such as differentiation of stem cells into cardiomyocyte-type cells to form new heart tissue in regenerative medicine [39].

Among others methods for cardiac cells alignment [40, 41], cardiac cells alignment by microprinted coating agents (chemical surface treatment) [42] and by topographical cues (topographical patterning) have been reported [43]. The cells aligned according to the cues exhibited a higher longitudinal velocity of action potential propagation [43].

HL-1 cells are cardiomyocytes isolated from AT-1 mouse atrial cardiomyocyte tumour lineage. HL-1 cells have some phenotype properties in common with cardiomyocytes, including beating activity. HL-1 cells can be serially passaged while still preserving their properties and beating activity [44]. These advantageous properties make HL-1 cells a suitable cardiac model for some cardiac studies, including electrophysiological studies [45]. The alignment possibilities of the HL-1 cells have been investigated in only a few studies [46, 47].

HL-1 cells have been selected as a model for alignment and proliferation, because they are able to be serially passaged and have a contractile ability, which allows the study of the electrophysiology of aligned HL-1 cells in future research. HL-1 cells proliferation is intended to reveal the effect of coating on HL-1 cell proliferation and the different affinity of the HL-1 cells for different substrates.

5.2 Materials and methods

5.2.1. Preparation of substrates

Substrates for HL-1 cells were fabricated by microfabrication methods. Briefly, substrates were 2 inch quartz wafers and 2 inch quartz wafers with thin layer of parylene C. Substrates were coated by photoresist, structure design was exposure by through a photolithographic mask and photoresist was developed. Then structures were etched by reactive ion etching (RIE) and photoresist was removed. All samples were cleaned by oxygen plasma. PDMS substrate with ridges was fabricated by mixing base polymer and hardener agent, pouring mixture onto the Si mould, left mixture to cure and peeling off PDMS from the Si mould.

The fabricated substrate was made with ridge heights of 0.3 µm, 1 µm and 3 µm. On each substrate, there were four blocks of ridges with width 2 µm, 4 µm, 8 µm and 16 µm. The width of the spaces between the ridges were same as the ridge widths. All these substrates were made for each material: Si, SiO_2, PDMS, parylene and parylene ridges on SiO_2 substrate. The scheme of fabricated substrates for the HL-1 cell alignment is presented in Figure 7.

Substrates for cell proliferation were made using the same process, but without ridge fabrication. A surface roughness for 1 µm deep etched areas and non-etched areas of substrates was measured via atomic force microscopy (AFM).

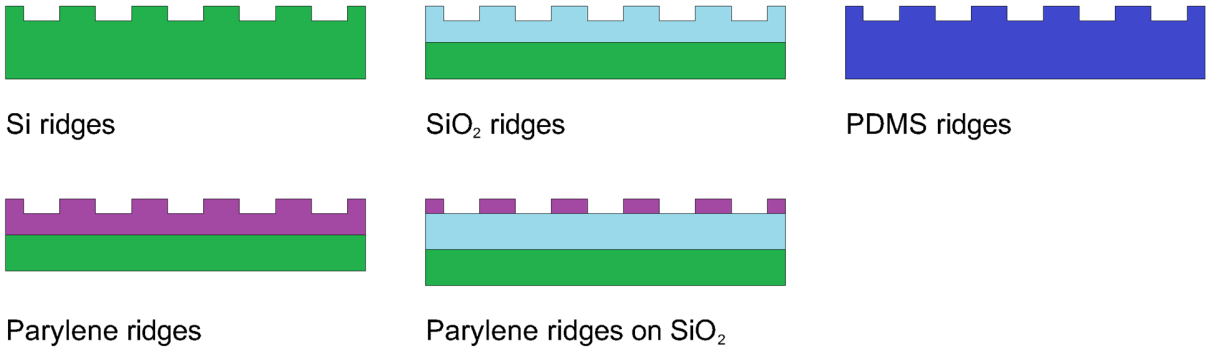

Figure 7: Substrates for the HL-1 cells alignment.

5.2.2. HL-1 cells seeding, cultivation, staining and visualisation

HL-1 cells cultivation was performed on the basis of published method [44]. Test substrates with ridges were used without coating, test substrates for cell proliferation were used coated by fibronectin diluted in gelatin from bovine skin and also without coating. HL-1 cells were seeded at a concentration of 7500 cell·cm^{-2} at all substrates and fixated after three days of cultivation. HL-1 cells for proliferation test were stained by DAPI (Sigma Aldrich, Czech Republic) and HL-1 cell for alignment test were stained with ActinGreen 488 ReadyProbes Reagent - A448 (Thermofisher, Czech Republic). Samples were observed by fluorescence microscope.

5.2.3. Image analysis and data analysis

The HL-1 cell proliferation was analysed by manual counting of the cells. The HL-1 cell alignment was analysed by prepared algorithm in the scripting programming language of the MATLAB programming environment. The input data is a fluorescence image of the HL-1 cells. According to whether a particular pixel crossed the threshold of green colour intensity, as well as the pixel's surroundings, the pixels are divided into five groups: pixels that are not cells, pixels that are inside of the cell borders, horizontal cell border pixels, vertical cell border pixels and transverse cell border pixels. The HL-1 cell alignment was calculated as a ratio of number of vertical border pixels to number of horizontal border pixels, as follows:

$$C_{align} = \frac{P_{vertical}}{P_{horizontal}} \quad (4)$$

where C_{align} is the cell alignment (-), $P_{vertical}$ is the number of vertical border pixels (-) and $P_{horizontal}$ is the number of horizontal border pixels (-).

5.4. Results and discussion

HL-1 cells concentration on various substrates after three days of cultivation in shown in Figure 8. Results show that coating supports HL-1 cells proliferation, however HL-1 cells grow well even on uncoated surfaces. This shows that HL-1 cells likely do not need surface coating before seeding on the substrate, and that the patterning of HL-1 cells by a chemical method with different material affinity would be difficult or not possible.

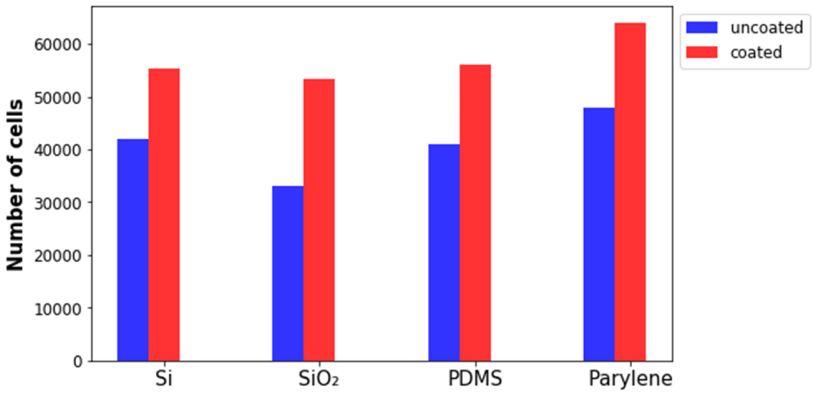

Figure 8: HL-1 cell concentration on various substrates after three days of cultivation.

HL-1 cells adhering on flat surfaces have a non-directional shape, while on the ridges, HL-1 cells have a longitudinal shape according to the direction of the ridges. The differences between HL-1 cells adhering on a flat surface, a surface with ridges and the edge of these surfaces are shown in Figure 9.

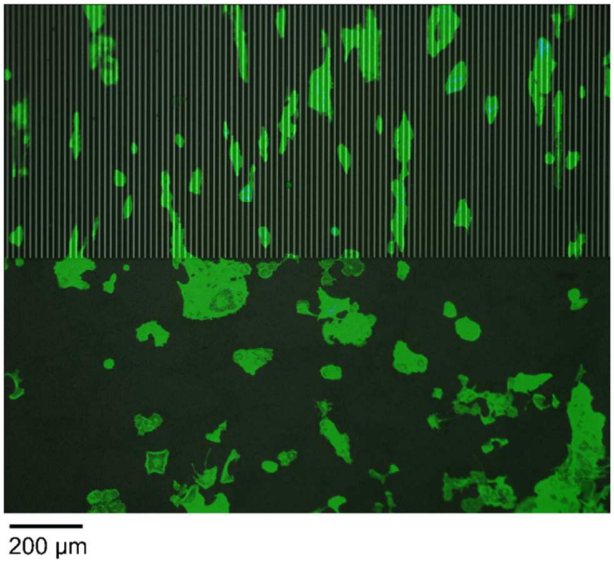

Figure 9: HL-1 cells on the edge of Si ridges 3 µm height and 8 µm wide. Bright field image overlaid by fluorescence image with partial transparency and increased colour saturation.

The HL-1 cells' alignment on the tested ridges is presented in Figure 10. The results show that the HL-1 cells alignment is better for higher ridges and narrow ridges (respectively, more ridges under the cell). Only exception is lower alignment of HL-1 cells on PDMS substrate with ridges 3 µm high and 2 µm wide. This is probably caused by PDMS hydrophobicity and too narrow gaps between ridges. Overly, the worst HL-1 cell alignment is found for the PDMS substrate with ridges, while the SiO_2 and Si substrates with ridges have more similar values and the best alignment was achieved by the HL-1 cell adhering on a parylene substrate with ridges. Another factor that can influence the HL-1 cell alignment is increased cell adhesion on rough surface [48, 49]. The surface roughness of tested substrates with ridges was measured by AFM,

and results are presented in Table 1. Significantly, the highest surface roughness was found for parylene, which also had the best HL-1 cell alignment.

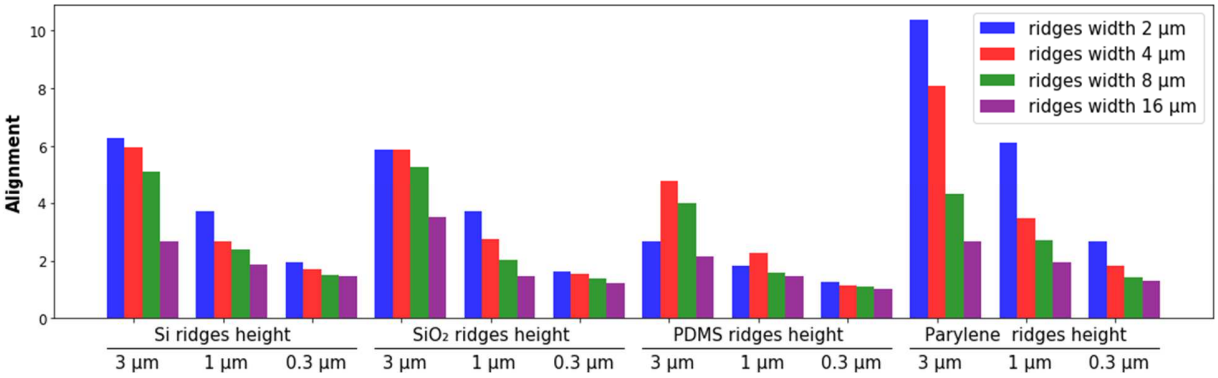

Figure 10: The HL-1 cells alignment on prepared substrates with ridges.

Table 1: The surface roughness on the top of the ridges, on the bottom between the ridges and their ratio. The surface roughness is defined for the ridges 1 µm high. For PDMS, data is already swapped, as the PDMS substrate with ridges was moulded from the Si master. The parylene non-etched surface was also shortly treated by oxygen plasma.

	Not etched	Etched	Ratio
Si	0.25 nm	0.74 nm	2.94
SiO_2	0.34 nm	0.92 nm	2.71
PDMS	0.35 nm	0.82 nm	2.36
Parylene	5.99 nm	23.09 nm	3.85

The possibility of chemical patterning of HL-1 cells was also tested. Parylene showed the best HL-1 cell alignment and the highest HL-1 cell proliferation, while SiO_2 showed the worst HL-1 cell proliferation. Therefore, a substrate was prepared with parylene ridges 0.3 µm high on the SiO_2 substrate in order to test whether the HL-1 cell alignment would significantly increase compared to ridges from other materials with the same height (0.3 µm). Results are shown in Figure 11. The parylene ridges on the SiO_2 substrate did not cause higher HL-1 cell compared to ridges of other materials. This allows to conclude that HL-1 cells alignment on parylene ridges on SiO_2 substrate is mainly caused by topographical factor, and that the effect of different chemical affinity is minimal.

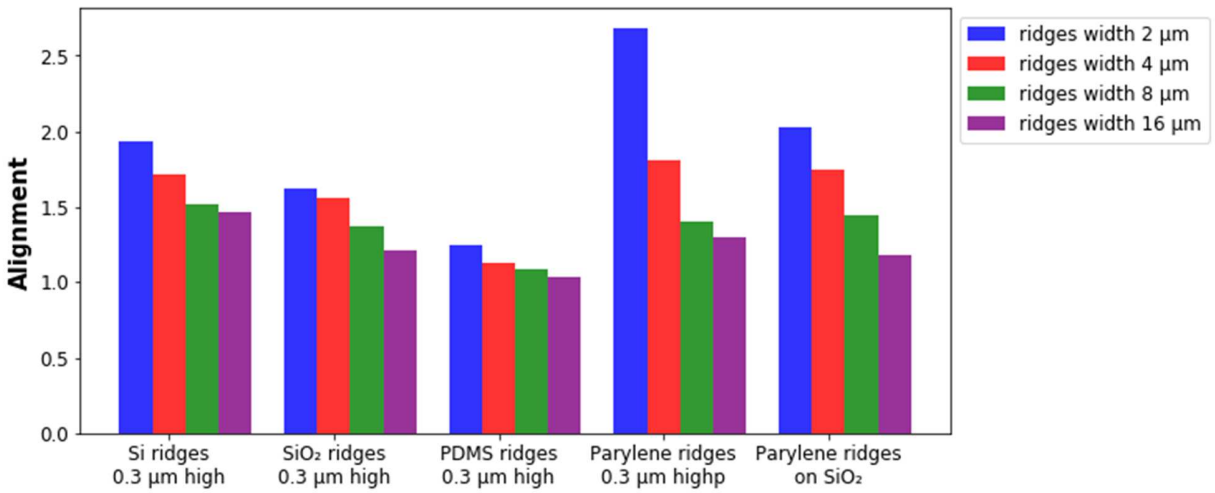

Figure 11: The HL-1 cells on substrates with ridges 0.3 µm height and parylene ridges on SiO_2.

6. Measurement of HL-1 cell field potential by MEA

6.1. Introduction

MEAs are widely used for *in vitro* applications in cardiophysiology. Primary cardiomyocytes isolated from neonatal organisms, cardiomyocyte derivative cells, stem cells and induced pluripotent stem cells differentiated into their cardiomyocyte subtypes can be cultured onto MEAs for a variety of purposes. These include characterization of cells electrophysiology, testing for drug use, investigation of the pharmacological effects of previously tested chemicals, among others.

HL-1 cells are easy to cultivate and they can be passaged while they maintain their spontaneous beating activity. This makes HL-1 cells useful for *in vitro* MEA studies of cardiac cell properties. HL-1 cells cultured on MEAs have been used as cardiac cell models [50-52] and also HL-1 cells have been used to demonstrate the possibility of electrophysiological measurements on MEAs [53, 54] and verify function of experimental MEA [55-57].

The aim is the fabrication of an MEA along with the seeding and cultivation of HL-1 cells on the MEA and measurement of the action potential of the cells. This will demonstrate the possibility of MEA fabrication as well as that of the measurement and analysis of HL-1 cell action potential.

6.2. Materials and methods

6.2.1. Fabrication of the MEA

Steps for the fabrication of the MEA are shown in Figure 12. In the end, MEA was diced in a 49 x 49 mm square, and a glass ring was glued onto the sample using PDMS. The lithographic design of the MEA and the fabricated MEA are shown in Figure 13. The MEA had dimensions 49 x 49 x 1 mm, 252 measure electrodes and 4 references electrode. Each measure electrode had measure area in shape of 100 µm square and the distances between the electrode centres were 250 µm.

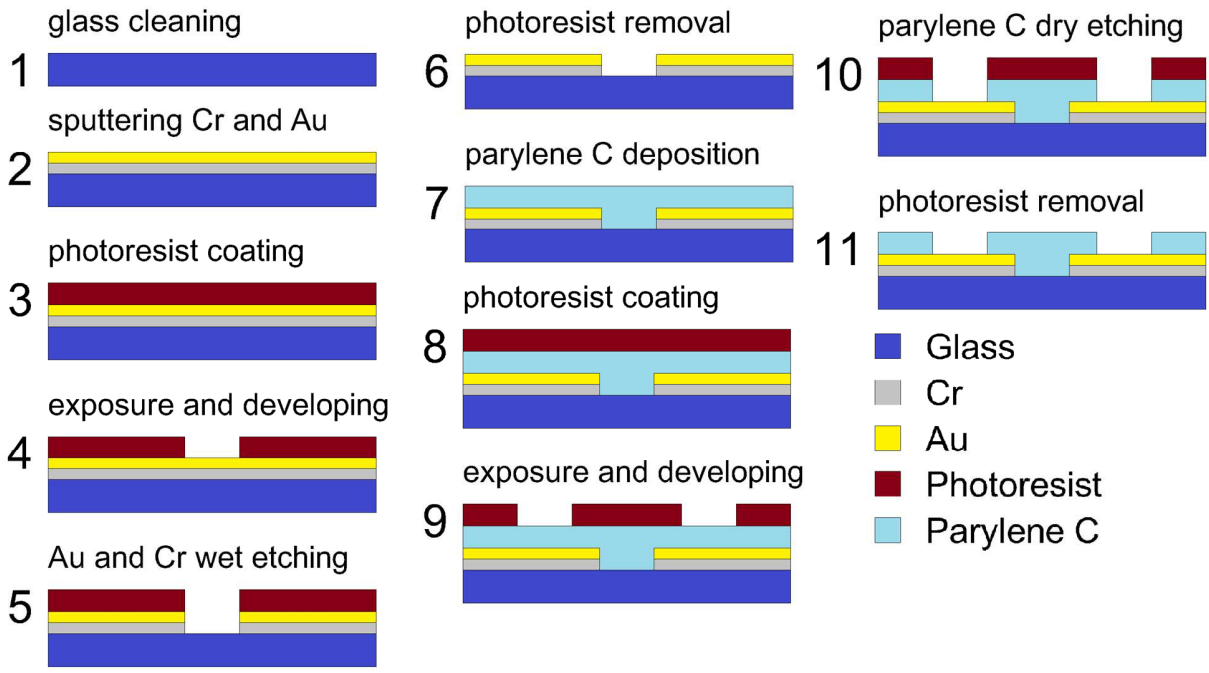

Figure 12: MEA fabrication steps.

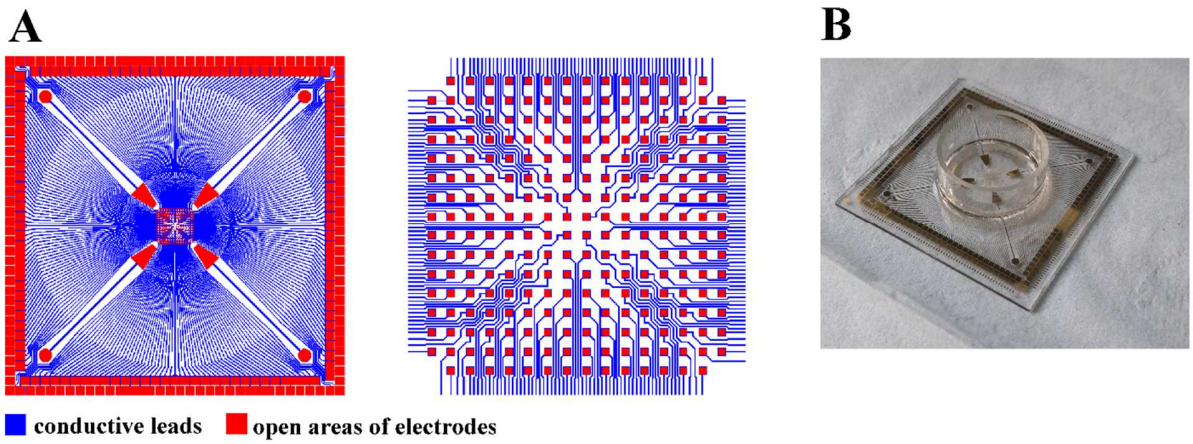

Figure 13: A: Design of the MEA and detail of the MEA middle area. B: Photo of the fabricated MEA.

6.2.2. MEA characterization

The impedances of the electrodes were measured using Autolab (PGSTAT204, Metrohm, Switzerland), and a 0.9% NaCl solution was used as an electrolyte. The main electrode of the MEA was its working electrode, while the Ag/AgCl was used as the reference electrode, and the Pt wire was used as the counter electrode. A 50 mV sine wave with a frequency range of 0.1–100 kHz was applied to analysed electrode, and measured impedances from the five electrodes were averaged.

6.2.3. Seeding and cultivation of the HL-1 cells on the MEA

HL-1 cells were cultivated according described method [44]. HL-1 cells were seeded on the MEA at a concentration of 7,500 cells·cm^{-2}. After 72 hours, the MEA seeded with the HL-1 cells was connected to a commercial measurement system (MEA2100-Systems, Multichannel Systems, Germany). Measurements were taken at room atmosphere while the MEA was heated to 37°C by an MEA2100 integrated heating element. The spontaneous activity of the HL-1 cells was measured using a commercial program (Multichannel Experimenter, Multichannel Systems, Germany) and analysed using a commercial program (Multichannel Analyzer, Multichannel Systems, Germany).

6.3. Results and discussion

The real part of impedance of MEA electrodes is a basic parameter for MEA characterisation. Electrodes with lower impedance have lower noise. Large electrodes have lower impedance than small electrodes, but large electrodes also record less localised information, making them more suitable for measuring cell populations rather than individual cells. Typical electrodes dimension for MEAs range approximately from 10–100 µm. The expected impedance value for electrodes with an unmodified surface is on the order of hundreds of kΩ. An impedance much lower than this can indicate problems with the insulation layer.

For a general comparison of the MEAs, a single impedance value is used for comparison. It is impedance measured at a 1 kHz and 50 mV sine wave in a 0.9% NaCl solution. The impedance of the Au electrodes was 120.4 kΩ. The impedance measurements are shown in Figure 14.

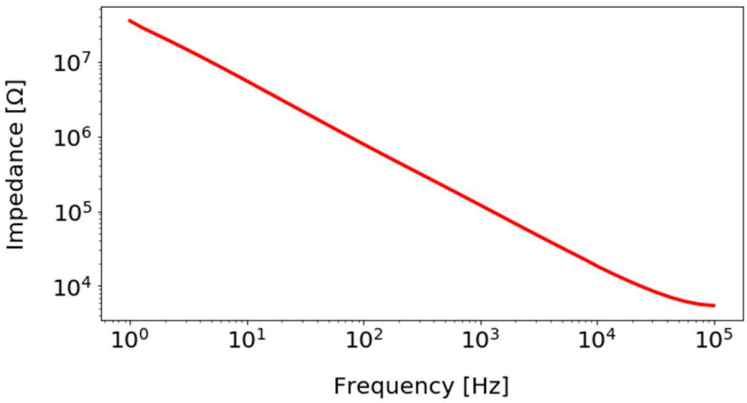

Figure 14: Real part impedance of Au electrodes of MEA.

HL-1 cells have the ability of spontaneous beating, the beat rate of each cell varies and this beat rate is called intrinsic frequency. Confluent HL-1 cells form gap junctions. An action potential is initiated at the cell with the highest intrinsic frequency and then spread by the gap junctions on other cells. The action potentials of the HL-1 cells were successfully recorded by the fabricated MEA. The measured action potentials are shown in Figure 15.

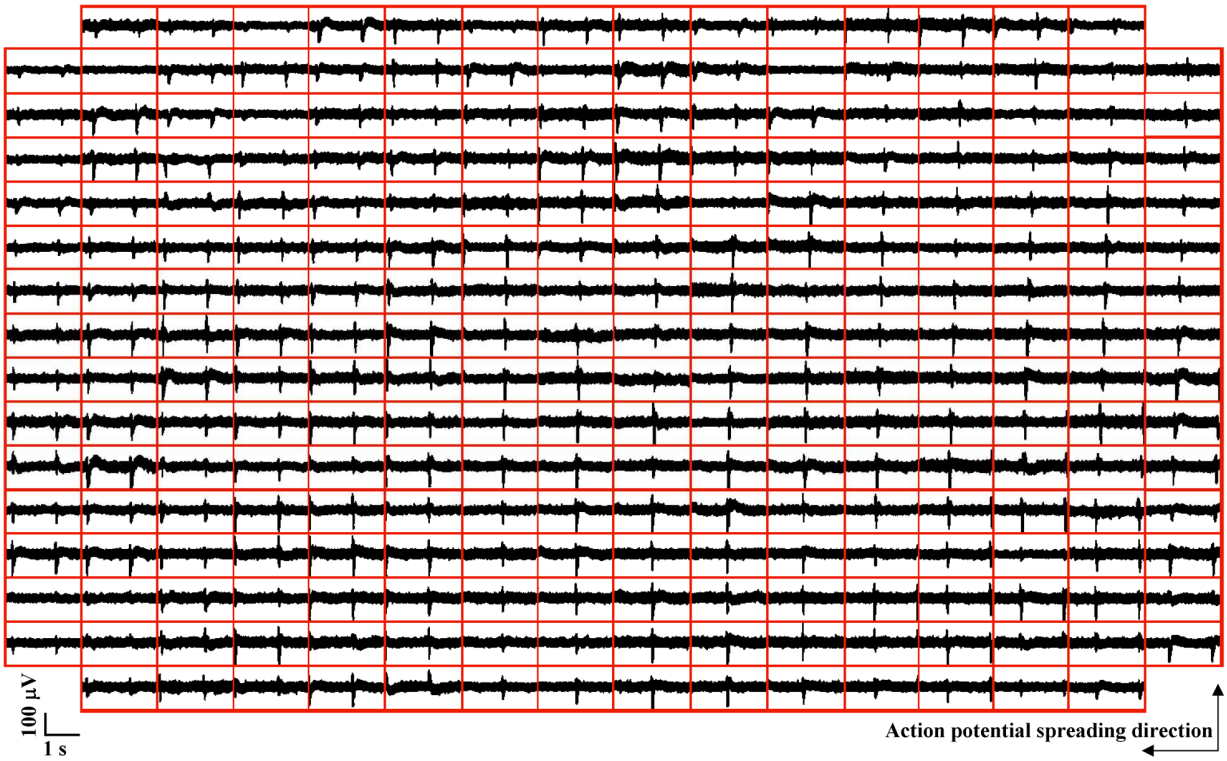

Figure 15: Measured action potentials of HL-1 cells.

MEA electrodes pick up electrical activity from the cells on their surfaces as well as from cells from their surroundings. Measured field potentials are made up of the contributions of many cells, and measured raw data show the shape of action potentials as a spike. Raw data can also be filtered to decrease the signal-to-noise ratio, allowing for more precise spike detection. In this study, the raw data was filtered through a high-pass filter, and spikes were detected when the signal exceeded the set threshold. To avoid multiple detections of the same spike, detection dead time was applied after spike detection. The filtrated signal allows for a more precise detection of spikes, but it also alters the shape of the spikes. Spike shape can generally be represented by the average signal from the raw signal of the detected spikes.

An example of the signal measured from one electrode is shown in Figure 16. For the raw signals, the average HL-1 peak from the upper amplitude to lower amplitude was 147.88 ± 37.72 µV and the noise was 12.07 ± 0.87 µV, calculated as mean absolute deviation (MAD) multiplied by 2. The raw signal for detection was filtered through both a low-pass (50 Hz) and a high-pass (5 Hz) filter. The beat rate of HL-1 cells was 65 bpm, and the action potential propagation was 4.4 $cm \cdot s^{-1}$. In other studies, beat rates of 65 bpm [50], 116 bpm [54], 165 - 204 bpm [55] and 60 bpm [56] have been measured. Action potential propagation speeds of 4.7 – 32 $cm \cdot s^{-1}$ [54], 1.6 – 1.9 $cm \cdot s^{-1}$ [55] and 0.1 $cm \cdot s^{-1}$ [56] have also been measured. This demonstrates that the vitality of HL-1 cells varies between laboratories.

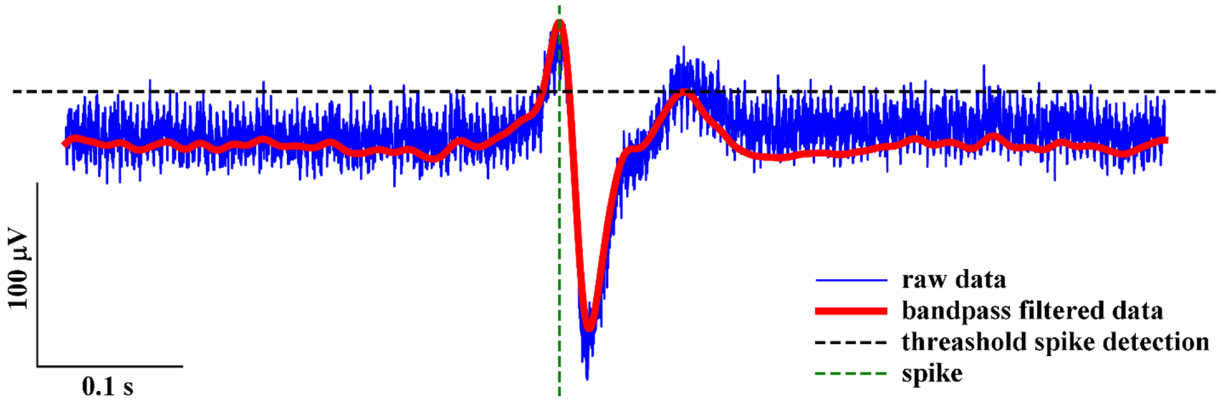

Figure 16: Example of the signal measured from one electrode.

7. MEA with a planar surface for cell patterning by microprinting

Partial results of the presented work in this chapter have been published in [58].

7.1. Introduction

MEAs have a specific application in combination with other contact techniques. A microfluidic culture platform for neuron culturing can be placed and aligned on a MEA surface where the microchannels allow neurites to grow and make defined interconnections. By specific design, it is possible to distinguish patterning axons from dendrites [59–63]. Cells that are seeded on MEA can be patterned by the microprinting method. Various coating agents and stamp dimensions were applied to form well-defined neural networks [64–68]. Cells that are not sensitive to the coating agent could be patterned by a combination of microprinting the coating agent and absorption of the antifouling agent [69, 70].

For these techniques would be advantageous to MEAs with a fully planar surface. PDMS structures must level down into the hole of the insulation layer onto the electrode surface; this creates defects on non-contacted surfaces. For instance, microprinting with a PDMS stamp on an MEA would leave unpatterned spaces on the edges of the insulation layer of electrodes, which would then be available for subsequent coating by the antifouling agent. The severity of the defect depends on the size of electrodes and the thickness of the insulation layer. If the electrodes and insulation layer are on one plane, the electrode's surface is then fully accessible without defects to the imprinting transfer process of the microprinting method and placing culturing platforms or microfluidic channels. MEAs with a fully planar surface would also avoid trapping air pockets during MEA positioning for in vivo applications [71].

Aim is development and optimization of fabrication process for MEA with fully planar surface, which is further called planar multi-electrode array (pMEA). The pMEA will be applied for measurement of HL-1 cells action potentials. The HL-1 cells will be patterned on pMEA surface by combination of microprinting with coating by anti-fouling agent, because previous study in chapter 5 shown that HL-1 cells cannot be patterned only by microprinting of coating agent.

7.2. Material and methods

7.2.1. The fabrication of pMEA

Steps for the fabrication of the pMEA are shown in Figure 17. The pMEA had dimensions 49 x 49 x 1 mm, 252 measure electrodes and 4 references electrode. Each measure electrode had measure area in shape of 100 µm square and the distances between the electrode centres were 300 µm.

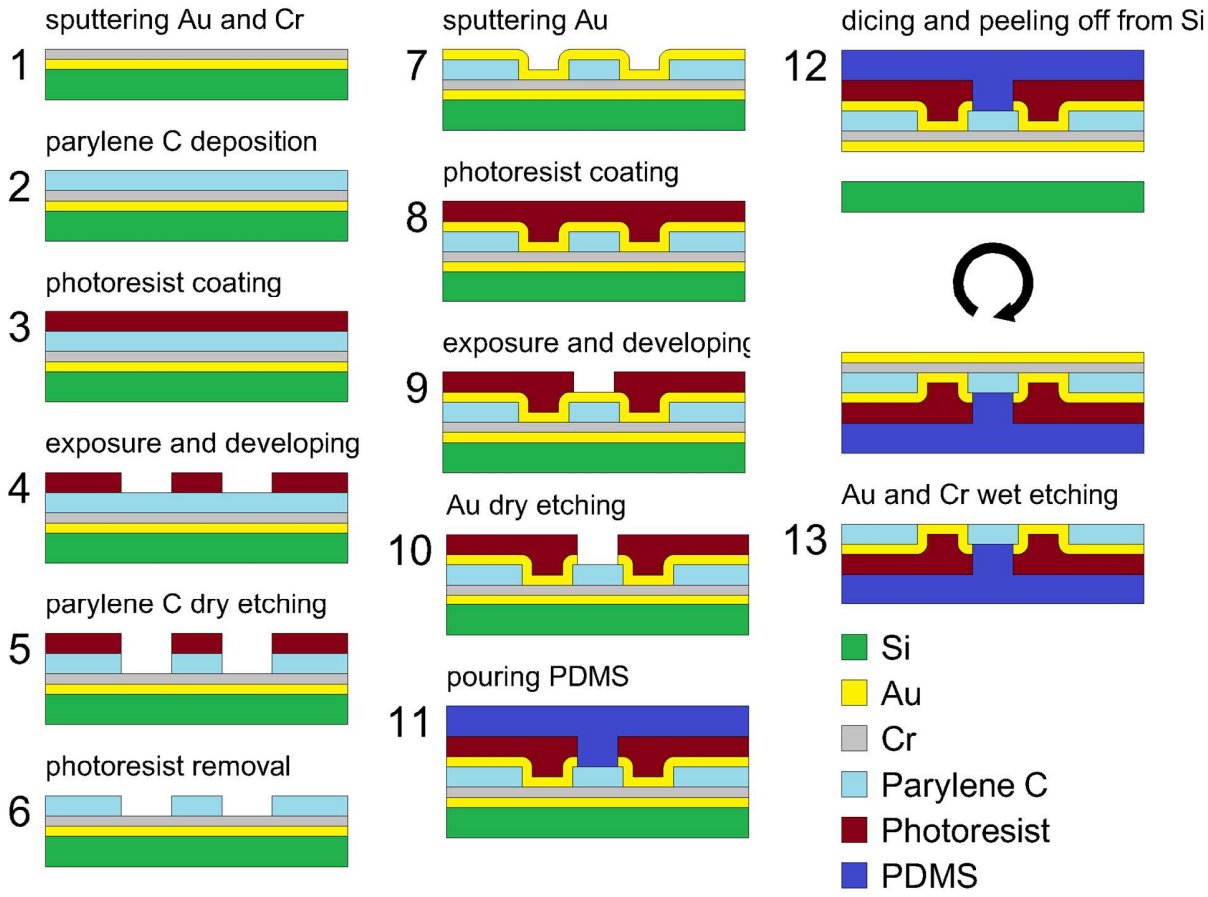

Figure 17. Fabrication steps of the pMEA.

7.2.2. Characterisation of planar electrodes

The profile of the sloped edge of the etched parylene C insulation layer was measured by a mechanical profilemeter (DektakXT, Bruker). The sloped edge of the insulation layer was measured from the bottom up, to ensure that the tip of stylus scanned the surface and not the stylus edge. The impedances of the electrodes were measured according method described in Chapter 6.2.2.

7.2.3. The fabrication of the PDMS stamp and microprinting method

Steps for the fabrication of the PDMS stamp and microprinting method shown in Figure 18.

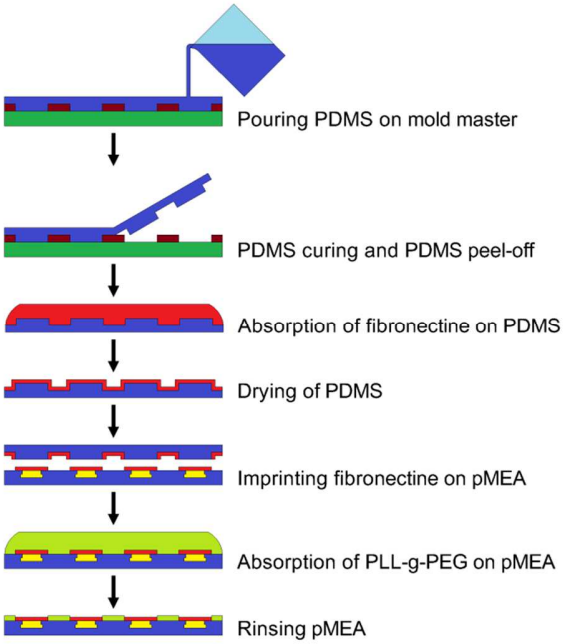

Figure 18. Scheme of microprinting of fibronectine and coating by PEG-g-PLL.

7.2.4. HL-1 cell culturing, measurements of action potentials, staining and visualisation

HL-1 cells were cultivated according described method [44]. HL-1 cells were seeded on the MEA at a concentration of 75,000 cells·cm^{-2}. After 24 hours, the MEA seeded with the HL-1 cells was connected to a commercial measurement system (MEA2100-Systems, Multichannel Systems, Germany). Measurements were taken at room atmosphere while the MEA was heated to 37°C by an MEA2100 integrated heating element. The spontaneous activity of the HL-1 cells was measured using a commercial program (Multichannel Experimenter, Multichannel Systems, Germany) and analysed using a commercial program (Multichannel Analyzer, Multichannel Systems, Germany). After the measurements, the HL-1 cells were fixed onto the pMEA, stained with ActinGreen 488 ReadyProbes Reagent - A448 and observed by fluorescence microscope.

7.3. Result and discussion

7.3.1 Optimize of fabrication of pMEA

Au serve as sacrificial peel off layer. It was sputtered at deposition rate 0.13 nm·s^{-1}. If deposition rate is too slow i.e. 0.04 nm·s^{-1}, Au will adhere on silicon surface strong enough, that weakest bond will be between PDMS and structures under it and it will peel off PDMS instead of Au. On the other hand, if Au deposition rate is too high i.e. 0.2 nm·s^{-1}, Au layer will leak up during parylene deposition and on surface of fabricated planar MEA will be dimples. Surface roughness of Au sacrificial layers was measured by AFM. The grains sizes were smaller for lower deposition rate, while the surface roughness decreased with increasing deposition rate. At deposition rate 0.04 nm·s^{-1} the surface roughness was 1.46 ± 0.17 nm with grain size 54.8 nm, at deposition rate 0.13 nm·s^{-1} the surface roughness was 1.23 ± 0.19 nm with grain size 48.4 nm and at deposition rate 0.2 nm·s^{-1} the surface roughness was 1.08 ± 0.16 nm with grain size

44.3 nm. At a high growth rate, the sputtered Au atoms are still moving on the substrate while new particles are sputtered. This causes stress in the interfacial region between the Au layer and the substrate and if the stress is too high, adhesion of the Au layer fails [72].

Electrodes have no adhesion layer. To increase electrodes durability, Au was sputtered at slow deposition rate. Durability will be also increase, if all open area of conductive Au layer, as are electrodes and pads, have edges buried under insulation layer. Electrodes will then withstand strong contact with PDMS stamp. After dry etching of Au layer to pattern electrodes, photo resist will carbonize and cannot be removed, however this do not affect functionality of pMEA.

After all structures are completed, on sample is poured PDMS, which serve as final pMEA substrate layer after silicon is peeled off. By peeling off, pMEA will turn upside down and lithographic design will be mirrored. From all structures weakest bond is between Au sacrificial layer and silicon. PMEA will peel off from silicon substrate with Au sacrificial layer. Scratches could easily appear on Au sacrificial layer by manipulation with sample by tweezers since Au sacrificial layer has very poor adhesion. If such scratches will appear on part of sample which will be peeled off, it will make successful peeling off more difficult or even impossible. PDMS is flexible material, with hardness shore A 48 [73], therefore it can be peeled off from silicon without dicing, however flexibility of PDMS is property with no advantage for MEA with *in vitro* application. A non-transparent MC35.1–W21 epoxy resin (ELCHEMCo, Czech Republic)(hardness shore D 90) has been successfully tested as the substitute. Because the epoxy resin stick harder on surface compare to PDMS, edges of silicon wafer needs to be diced before peeling off planar MEA to reveal Au sacrificial layer.

A SEM picture of the fabricated planar electrode is shown in Figure 19.

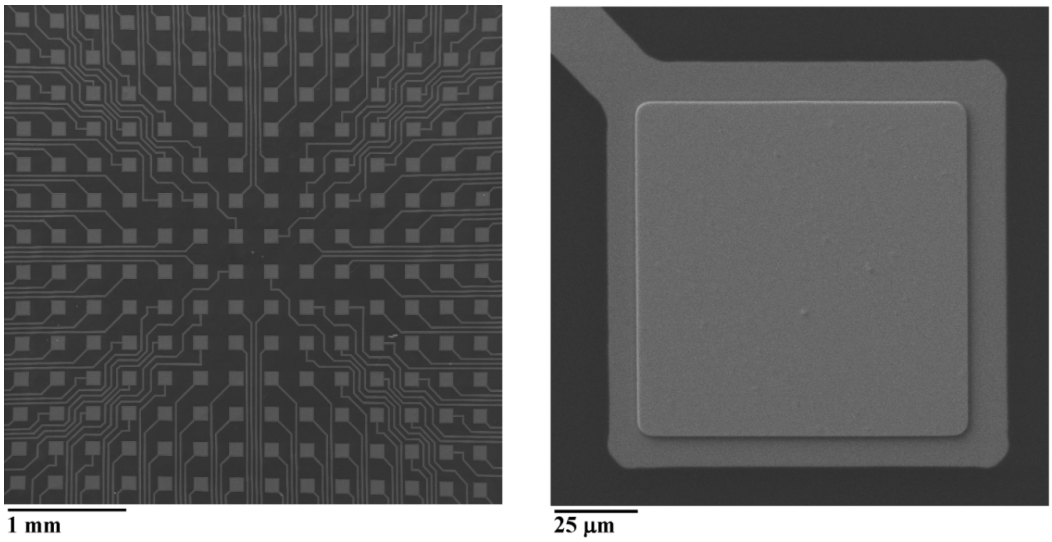

Figure 19. On the left, the SEM picture of the pMEA. On the right, the SEM picture of the planar electrode.

7.3.2. The profile of the sloped edge of the insulation layer and the impedance of the planar electrodes

The expected value of impedance for electrodes with an unmodified surface is hundreds of kΩ. However, the conductive layer of the pMEA is led across the sloped edge of the insulating layer, where the conductive layer is thinner. This reduces the conductivity and increases impedance. Therefore, the RIE of parylene C was done at high pressure (200mTorr) to achieve a high under-etched edge of the insulation layer, so creating a flattened profile. The profile of the sloped edge of the insulation layer was measured by a mechanical profilemeter following fabrication step 6 from Figure 17. The profile was not linear. The sharpest slope in the profile was at the bottom edge of the insulation layer, where the angle measured 32°. The whole profile is shown in Figure 20A. The measured real part of impedance of the pMEA is shown in Figure 20B. The impedance at 1 kHz for the pMEA was 136 kΩ. Leading electrodes across the flattened sloped edge of the insulation layer did not significantly affect the impedance of electrodes.

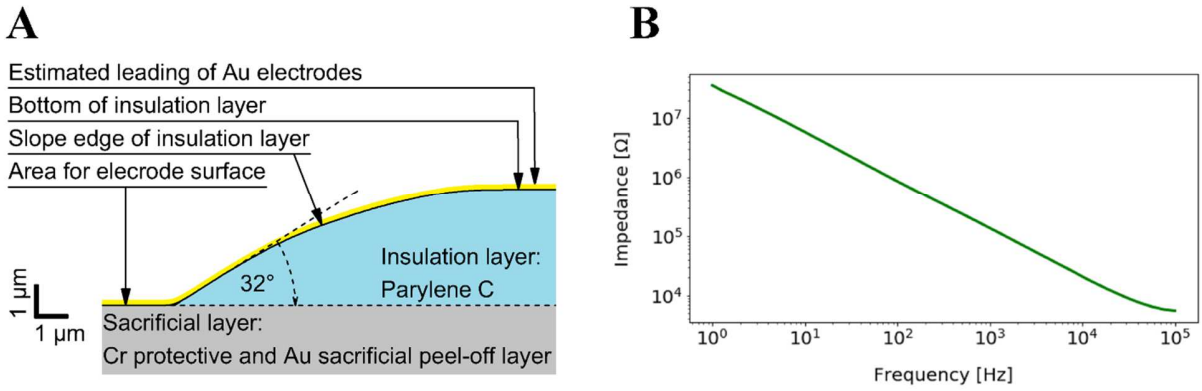

Figure 20. A: The profile of the sloped edge of the insulation layer. B: Real part of impedance of the pMEA electrodes.

7.3.3. Cell patterning on pMEA by microprinting

Microprinting with a PDMS stamp is a well-described method [74, 75]. The height of the raised features 24 µm was sufficient to avoid roof collapse of the PDMS stamp. The pressure applied to the PDMS stamp was 25 kPa. However, the pressure applied on the PDMS stamp and the length (time) of the pressure are not critical parameters for successful imprinting of the fibronectin. According to preliminary experiments from chapter 5, HL-1 cells grow well on various surfaces (silicon, glass, PDMS, parylene C) even without coating. Patterning HL-1 cells just by imprinting of fibronectin is not possible. Therefore, for patterning was used a combination of the microprinting method with an antifouling agent coating. The antifouling agent was used poly-ethylene glycol (PEG). PEG is a polynonionic polymer of a polyether compound that blocks biological recognition as is cell adhesion. To allow adherence to a surface, the PEG is synthesised as a copolymer with poly-L-lysine (PLL). The structure of the copolymer is comb, with a positively charged PLL backbone that adheres to a negatively charged surface while the chains of PEG are exposed to the surroundings. Therefore, the cell cannot adhere to a surface coated by PLL-g-PEG [76]. To enhance PLL-g-PEG adhesion, the surface can be treated with oxygen plasma, but only for a short time, since oxygen plasma also etches parylene C. Parylene C treated by plasma will remain oxidised over time [77, 78] unlike other commonly-used materials such as glass or PDMS.

7.3.4. A measure of HL-1 cells action potential on the pMEA

The scheme of expected alignment of HL-1 cells on the pMEA is shown in Figure 21. After 24 hours, fully confluent HL-1 cells already form gap junctions while they are still patterned in lines. The cells in lines present their individual spontaneous and synchronous beating activity. Each line has an individual beat rate corresponding to an individual peace marker cell with the highest intrinsic frequency. For raw signal, the average HL-1 peak from upper amplitude to lower amplitude was 163.09 ± 42.96 µV and noise was 11.27 ± 0.66 µV calculated as 2·MAD. The propagation velocities of action potentials were defined as the distance between the detected thresholds of peaks. The direction of action potential propagation was also individual for HL-1 cells patterned in lines. It was analysed action potential propagation velocities in four clearly defined HL-1 cell columns, marked as A, B, C, and D in Figure 22. The velocities of the action potential propagation were: A – 7.18 mm mm·s^{-1}, B – 7.29 mm·s^{-1}, C – 6.27 mm·s^{-1}, D – 6.68 mm·s^{-1}. HL-1 cells were fixed, stained, visualised after the measurement and it is shown at Figure 23.

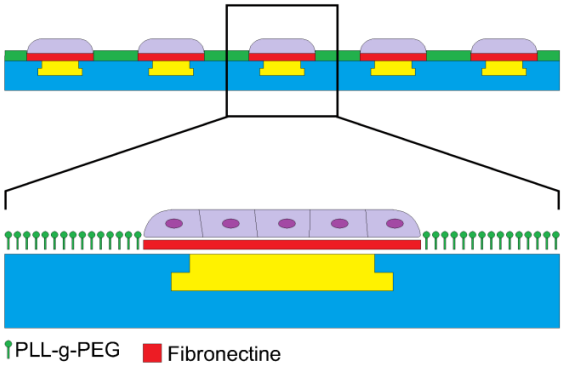

Figure 21. The scheme of HL-1 cells patterned on planar electrodes.

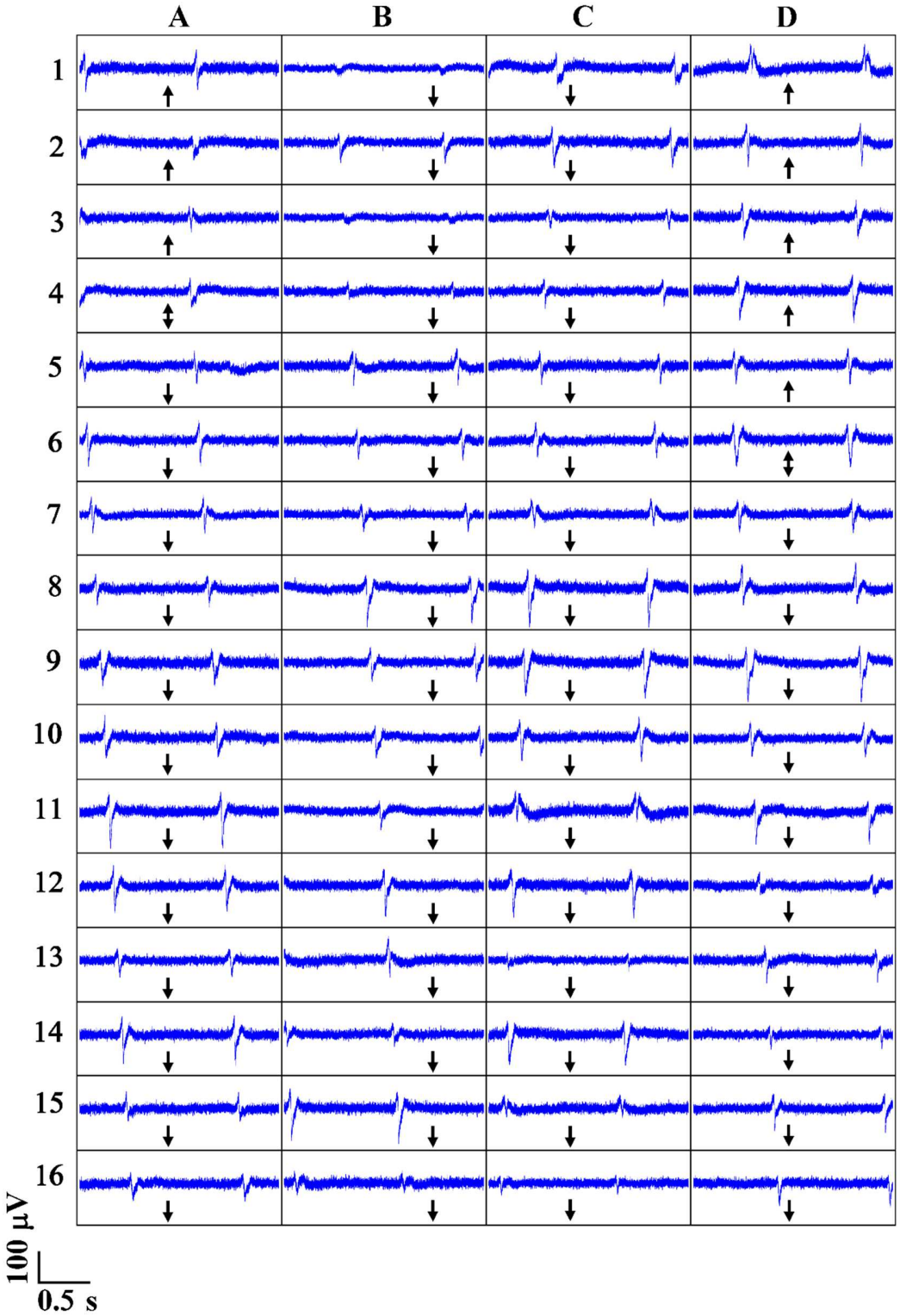

Figure 22. HL-1 cells action potential propagation over the electrodes of the pMEA. The HL-1 grows in separated lines with their individual beating activity. Arrows shows direction of action potential propagation.

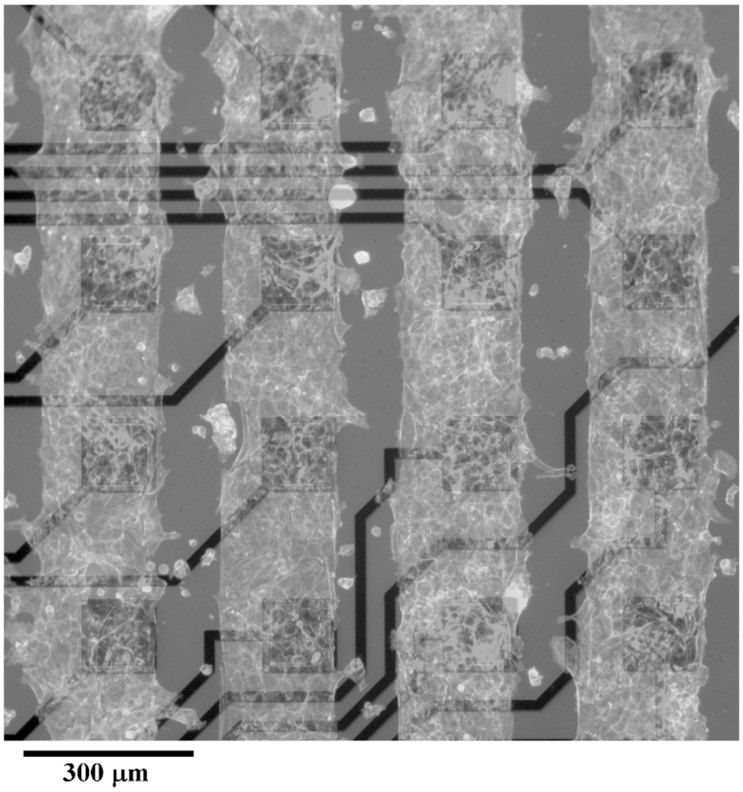

Figure 23. A fluorescent image of the planar electrodes with patterned HL-1 cells overlapped by a partially transparent corresponding bright-field image to highlight the electrodes' positions.

8. Conclusion

This work presents fabrication technology of pMEA for effective patterning of excitable cells by microprinting method combined with coating by antifouling agent. The work also presents effectiveness of patterning of embryonic hippocampal neurons and cardiac-like HL-1 cells by topographical patterning and chemical patterning.

Testing structures for neurons and HL-1 cells patterning were fabricated. Fabricated ridges are structures, which are similar to extracellular matrix scaffold on which neurons grow *in vivo*. Neurons' morphology, including long axons, makes them unique cells for alignment. Neurons growing on fabricated ridges shown tendency align longitudinally according to ridges direction and also much lower tendency of alignment in vertical direction. Neurons alignment effectivity increase with ridges height and the distance between the ridges should increase with the ridges height. For chemical patterning, neurons shown stronger affinity to parylene structures than the quartz substrate and that makes parylene effective material for neurons patterning. HL-1 cells also aligned longitudinally according to ridges direction, but they are not sensitive for chemical patterning. HL-1 cells adhered well on coated and uncoated surfaces and so HL-1 cells did not have higher affinity to parylene structures.

Before excitable cells patterning on MEA, the fabrication of MEA with conventional design, characterization of MEA parameters and cell action potential measurement had to be done. A number of MEA with conventional design have been made by different fabrication technologies in order to analyse

MEA properties and record electrical activity of excitable cells. One of these technologies was demonstrated in this work. HL-1 cells were used as excitable cells for measurement of electrical activity by fabricated MEA.

Design of pMEA and alignment of cells on the pMEA was based on obtained results of cells alignment and MEA fabrication technologies. The pMEA have fully planar surface which is advantageous for cell patterning by microprinting methods, especially combined with antifouling agent. The pMEA could be further advantageous for placing culturing platforms or microfluidic channels on its surface and to avoid forming air pockets during MEA positioning on tissue for *in vivo* applications.

The pMEA was fabricated by special fabrication process. Briefly, the substrate was silicon wafer on which was sputtered Au sacrificial peel-off layer and Cr. Then it was deposited insulation layer, electrodes and PDMS was poured on sample as second substrate. PMEA was fabricated in reverse order from top layer to bottom layer. After dicing, pMEA was simply peeled-off from silicon substrate due low adhesion between the Au sacrificial peel-off layer and the silicon substrate. The Au sacrificial peel-off layer must be sputtered at correct deposition rate, because too slow deposition leads to good adhesion between the Au sacrificial peel-off layer and silicon, therefore peeling-off would not be successful and too high deposition rate leads to low quality of Au sacrificial peel-off layer, which can be damaged during fabrication processing of pMEA. The advantage of using the Au sacrificial peel-off layer is that device is immediately released from substrate. The pMEA is flexible what have no advantage for *in vitro* application, but PDMS as substrate can be substituted by epoxy resin, which is solid after curing.

Because HL-1 cells are not sensitive to chemical patterning, the microprinting method by itself cannot be used to pattern HL-1 cells. But HL-1 cell will not adhere on surface coated by antifouling agent, which prevents adhesion of cells of any type. As antifouling agent was used PEG. PEG can be well coated only on surface treated by oxygen plasma, so PEG can be patterned by previous microprinting of fibronectine (or other agent) and PEG will coat not microprinted patterns. HL-1 cells were patterned on pMEA by combination of microprinting and coating by antifouling agent. HL-1 cells were patterned into the strips and electrical activity was analysed.

MEA allows to perform electrophysiological experiments with excitable cells on its surface. Patterning and alignment cells on MEA, allows formation of defined cells connections, which can be used to formation of working systems or for better isolation of analysed parameters. Neurons have great potential for patterning on MEA, however no experiments with neurons and MEA were done, because availability of neurons was limited. Therefore HL-1 cells were used for pMEA testing.

References:

[1] SHERWOOD, L. *Human Physiology - From Cells to Systems*. Florence, United States: Cengage Learning, Inc, 2015. ISBN 978-1-28586-693-2.

[2] MARIEB, E. N. and HOEHN, K. *Human anatomy and physiology*. Harlow, United Kingdom: Pearson Education Limited, 2018. ISBN 0-321-74326-1.

[3] KATZ, A. M. *Physiology of the Heart*. Philadelphia, United States: Lippincott Williams and Wilkins, 2005. ISBN 978-1-60831-171-2.

[4] SCHLÜTER, K. D. *Cardiomyocytes – Active Players in Cardiac Disease*. Cham, Switzerland: Springer International Publishing AG, 2016. ISBN 978-3-319-31249-1.

[5] LEVICK, J. R. *An Introduction to Cardiovascular Physiology*. Londod, England: Butterworth & Co, 1991. ISBN 0-750-61028-X.

[6] ZANA, A., ROSEN M. R. *An Introduction to Cardiac Electrophysiology.* Chur, Switzerland: Harwood-Academic Publishers, 2005. ISBN 90-5702-457-8.

[7] PURVES, D. et al. *Neuroscience*. Sunderland, United States: Sinauer Associates Inc., U.S., 2008. ISBN 978-0-878-93697-7.

[8] BOYETT, M. R., HONJO, H and KODAMA, I. The sinoatrial node, a heterogeneous pacemaker structure. *Cardiovascular Research*, 2000, vol. 47, pp. 658-687. ISSN 0008-6363.

[9] SHEIKH, F., ROSS, R. S. and CHEN, J. Cell-Cell Connection to Cardiac Disease. Trends in Cardiovascular Medicine, 2009, vol. 19, no. 6, pp. 182-190. ISSN 1050-1738.

[10] KLEBÉR A. G. et al. Changes in conduction velocity during acute ischemia in ventricular myocardium of the isolate porcine heart. *Circulation*, 1986, vol. 73, no. 1, pp. 189-198. ISSN 0009-7322.

[11] SPACH, M. S. et al. The discontinuous nature of propagation in normal canine cardiac muscle. Evidence for recurrent discontinuities of intracellular resistance that affect the membrane currents. *Circulation Research*, 1981, vol. 48, no. 1, pp. 39-54. ISSN 0009-7330.

[12] TRACY, R. E., SANDER. G. E. Histologically Measured Cardiomyocyte Hypertrophy Correlates with Body Height as Strongly as with Body Mass Index. *Cardiology Research and Practice*, 2011. ISSN 2090-8016.

[13] LI, Y. et al. Engineering cell alignment in vitro. *Biotechnology Advances*, 2014, vol. 32, no. 2, pp. 347-365. ISSN 0734-9750.

[14] YAN, L., ZHAO, X. M. and WHITESIDES, G. M. Patterning a Preformed, Reactive SAM Using Microcontact Printing. *Journal of the American Chemical Society*, 1998, vol. 120, no. 24, pp. 6179-6180. ISSN 0002-7863.

[15] NIKKHAH, M. et al. Engineering microscale topographies to control the cell–substrate interface. Biomaterials, 2012, vol. 33, no. 21, pp. 5230-5246. ISSN 0142-9612.

[16] OBIEN, M. E. et al. Revealing Neuronal Function Through Microelectrode Array Recordings. *Frontiers in Neuroscience*, 2015, vol. 8, pp. 1-30. ISSN 1662-453X.

[17] SPIRA, M. E. and HAI, A. Multi-Electrode Array Technologies For Neuroscience And Cardiology. *Nature Nanotechnology*, 2013, vol. 8, pp. 83-94. ISSN 1748-3387.

[18] SLAVÍK, J. et al. Hippocampal neurons patterning on quartz grooves and parylene cues on quartz substrate. *Applied Sciences*. ISSN 2076-3417. (Submitted publication)

[19] HATTEN, M. E. Riding the glial monorail: a common mechanism for glial-guided neuronal migration in different regions of the developing mammalian brain. *Trends Neuroscience*, 1990, vol. 13, no. 5, pp. 179-184. ISSN 0166-2236.

[20] RAKIC, P. Mode of cell migration to the superficial layers of fetal monkey neocortex. *The Journal of Comparative Neurology*, 1972, vol. 145, no. 1, pp. 61-83. ISSN 1096-9861.

[21] O'ROURKE, N. A. et al. Tangential migration of neurons in the developing cerebral cortex. *Development*, 1995, vol. 121, no. 7, pp. 2165-2176. ISSN 0950-1991.

[22] HYNES, R. O., PATEL, R. and MILLER, R. H. Migration of neuroblasts along preexisting axonal tracts during prenatal cerebellar development. *Journal of Neuroscience*, 1986, vol. 6, no. 3, pp. 867-876. ISSN 0270-6474.

[23] JACOBS, J. R. and GOODMAN, C. S. Embryonic development of axon pathways in the Drosophila CNS. I. A glial scaffold appears before the first growth cones. *Journal of Neuroscience*, 1989, vol. 9, no. 7, pp. 2402-2411. ISSN 0270-6474.

[24] SILVER, J. and SIDMAN, R. L. A mechanism for the guidance and topographic patterning of retinal ganglion cell axons. *The Journal of Comparative Neurology*, 1980, vol. 189, no. 1, pp. 101-111. ISSN 1550-7149.

[25] KRAYANEK, S. and GOLDBERG, S. Oriented extracellular channels and axonal guidance in the embryonic chick retina. *Developmental Biology*, 1981, vol. 84, no. 1, pp. 41-50. ISSN 0012-1606.

[26] SCHMIDT, C. E. and LEACH, J. B. Neural tissue engineering: strategies for repair and regeneration. *Annual Review of Biomedical Engineering*, 2003, vol. 5, pp. 293-347. ISSN 1523-9829.

[27] LI, G. N. and HOFFMAN-KIM, D. Tissue-engineered platforms of axon guidance. *Tissue Engineering Part B: Reviews*, 2008, vol. 14, no. 1, pp. 33-51. ISSN 1937-3368.

[28] HOFFMAN-KIM, D., MITCHEL J. A. and BELLAMKONDA, R. V. Topography, cell response, and nerve regeneration. *Annual Review of Biomedical Engineering*, 2010, vol. 12, pp. 203-231. ISSN 2152-4955.

[29] HIRONO, T. et al. Recognition of artificial microstructures by sensory nerve fibers in culture. *Brain Research*, 1988, vol. 446, no. 1, pp. 189-194. ISSN 0006-8993

[30] CLARK, P. et al. Topographical control of cell behaviour: II. Multiple grooved substrata. *Development*, 1990, vol. 108, no. 4, pp. 635-644. ISSN 0950-1991.

[31] JOHANSSON, F. et al. Axonal outgrowth on nano-imprinted patterns. *Biomaterials*, 2006, vol. 27, no. 8, pp. 1251-1258. ISSN 0142-9612.

[32] STEPIEŃ, E., STANISZ, J. and KOROHODA, W. Contact guidance of chick embryo neurons on single scratches in glass and on underlying aligned human skin fibroblasts. *Cell Biology International*, 1999, vol. 23, no. 2, pp. 105-116. ISSN 1065-6995.

[33] NAGATA, I. and BAKATSUJI, N. Rodent CNS neuroblasts exhibit both perpendicular and parallel contact guidance on the aligned parallel neurite bundle. *Development*, 1991, vol. 112, no. 2, pp. 581-590. ISSN 0950-1991

[34] NAGATA, I., KAWANA, A. and NAKATSUJI, N. Perpendicular contact guidance of CNS neuroblasts on artificial microstructures. *Development*, 1993, vol. 117, no. 1, pp. 401-408. ISSN 0950-1991.

[35] RAJNICEK, A., BRITLAND, S. and McCAIG, C. Contact guidance of CNS neurites on grooved quartz-influence of groove dimensions neuronal age and cell type. *Journal of Cell Science*, 1997, vol. 110, pp. 2905-2913. ISSN 0021-9533

[36] BEAUDOIN G. M. J. et al. Culturing pyramidal neurons from the early postnatal mouse hippocampus and cortex. Nature Protocols, 2012, vol. 7, no. 9, pp. 1741-1754. ISSN 1754-2189.

[37] BIL'DIUG, N. B. and PINAEV, G. P. Extracellular matrix dependence of the cardiomyocyte contractile apparatus organization. *Tsitologiia*, 2013, vol. 55, no. 10, pp. 713-724. ISSN 0041-3771.

[38] NAG, A. C. and CHENG, M. Adult mammalian cardiac muscle cells in culture. Tissue and Cell, 1981, vol. 13, no. 3, pp. 515-523. ISSN 0040-8166.

[39] LEOR, J., AMSALEM, Y. and COHEN, S. Cells, scaffolds, and molecules for myocardial tissue engineering. *Pharmacology & Therapeutics*, 2005, vol. 105, no. 2, pp. 151.163. ISSN 0163-7258.

[40] FINK, C. et al. Chronic stretch of engineered heart tissue induces hypertrophy and functional improvement. *The FASEB Journal*, 2000, vol.14, no. 5, pp. 669-679. ISSN 0892-6638.

[41] RADISIC, M. et al. Functional assembly of engineered myocardium by electrical stimulation of cardiac myocytes cultured on scaffolds. *Proceedings of the National Academy of Sciences of the United States of America*, 2004, vol. 101, no. 52, pp. 18129-18134. ISSN 0027-8424.

[42] BURSAC, N. et al. Cardiomyocyte cultures with controlled macroscopic anisotropy: a model for functional electrophysiological studies of cardiac muscle. *Circulation Research*, 2002, vol. 91, no. 12, pp. 45-54. ISSN 0009-7330.

[43] KIM, D. H. et al. Nanoscale cues regulate the structure and function of macroscopic cardiac tissue constructs. *Proceedings of the National Academy of Sciences of the United States of America*, 2010, vol. 107, no. 2, pp. 565-570. ISSN 0027-8424.

[44] CLAYCOMB, W. C. et al. HL-1 cells: a cardiac muscle cell line that contracts and retains phenotypic characteristics of the adult cardiomyocyte. *Proceedings of the National Academy of Sciences of the United States of America*, 1998, vol. 95, no. 6, pp. 2979-2984. ISSN 0027-8424.

[45] WHITE, S. M., CONSTANTIN, P. E. and CLAYCOMB, W. C. Cardiac physiology at the cellular level: use of cultured HL-1 cardiomyocytes for studies of cardiac muscle cell structure and function. *American Journal of Physiology-Heart and Circulatory Physiology*, 2004, vol. 286, no. 3, pp. 823-829. ISSN 03636135.

[46] GONNERMAN, E. A. et al. The promotion of HL-1 cardiomyocyte beating using anisotropic collagen-GAG scaffolds. Biomaterials, 2012, vol. 33, no. 34, pp. 8812-8821. ISSN 0142-9612.

[47] ZHAO, K. et al. HL-1 Cardiomyocyte Mechanistic Responses to Micro-Patterned Culture Environment. In: *10th IEEE international Conference on Nano/Molecular Medicine and Engineering*: 30-2. November 2016. Macau, China: IEEE 2016.

[48] XU, Ch. et al. *In vitro study of human vascular endothelial cell function on materials with various surface roughness*. Journal of Biomedical Materials Research - Part A, 2004, vol. 71, no. 1, pp 154-161. ISSN 1552-4965.

[49] HALLAB, N. J. et al. *Evaluation of Metallic and Polymeric Biomaterial Surface Energy and Surface Roughness Characteristics for Directed Cell Adhesion*. Tissue Engineering, 2004, vol. 7, no. 1, pp. 55-71. ISSN 2152-4947.

[50] LAW, J. K. et al. The use of microelectrode array (MEA) to study the protective effects of potassium channel openers on metabolically compromised HL-1 cardiomyocytes. *Physiological Measurement*, 2009, vol. 30, no. 2, pp. 155-167. ISSN 0967-3334.

[51] LAW, S. H. et al. An Updated Review of Lysophosphatidylcholine Metabolism in Human Diseases. *International Journal of Molecular Sciences*, 2019, vol. 20, no. 5. ISSN 1422-0067.

[52] LIU, E., GOLDHABER, J. I. and WEISS, J. N. Effects of lysophosphatidylcholine on electrophysiological properties and excitation-contraction coupling in isolated guinea pig ventricular myocytes. *Journal of Clinical Investigation*, 1991, vol. 88, no. 6, pp. 1819-1832. ISSN 0021-9738.

[53] MEYER, T., KRAUSHAAR, U. and GUENTHER, E. Microelectrode Array (MEA) high resolution electrophysiological mapping of cardiac cell, tissue and organ preparations. In: *World Congress on Medical Physics and Biomedical Engineering: 7-12. September 2009. Munich, Germany*: Springer, Berlin, Heidelberg, 2009, pp. 112-115. ISBN 978-3-642-03886-0.

[54] GARMA, L. D. et al. Cost-effective and multifunctional acquisition system for in vitro electrophysiological investigations with multi-electrode arrays. *PLoS ONE*, 2019, vol. 14, no. 3. ISSN 1932-6203.

[55] GIOVANGRANDI, L. et al. Low-cost microelectrode array with integrated heater for extracellular recording of cardiomyocyte cultures using commercial flexible printed circuit technology. *Sensors and Actuators B*, 2006, vol. 113, pp. 545–554. ISSN 0924-4247.

[56] KIREEV, D. et al. Graphene Multielectrode Arrays as a Versatile Tool for Extracellular Measurements. *Advanced Healthcare Materials*, 2017, vol. 12, no. 6. ISSN 2192-2659.

[57] SANTORO, F. et al. On Chip Guidance and Recording of Cardiomyocytes with 3D Mushroom-Shaped Electrodes, Nano letters, 2013, vol. 13, no. 11. ISSN 1530-6984.

[58] SLAVÍK, J. et al. Multi-electrode array with a planar surface for cell patterning by microprinting. Sensors, 2019, vol. 19, no. 24, p. 1-11. ISSN: 1424-8220.

[59] DEGENAAR, P. et al. Method for Micrometer Resolution Patterning of Primary Culture Neurons for SPM Analysis. *Journal of Biochemistry*, 2001, vol. 130, no. 3, pp. 367-376. ISSN 1756-2651.

[60] GRISCOM, L. et al. Techniques for patterning and guidance of primary culture neurons on micro-electrode arrays. *Sensors and Actuators B: Chemical*, 2002, vol. 83, no. 1-3, pp 15-21. ISSN 0925-4005.

[61] MORIN, F. Constraining the connectivity of neuronal networks cultured on microelectrode arrays with microfluidic techniques: a step towards neuron-based functional chips. *Biosensors and Bioelectronics*, 2006, vol. 21, no. 7, pp. 1093-1100. ISSN 0956-5663.

[62] TAYLOR, A. M. et al. A microfluidic Culture Platform For CNS Axonal Injury, Regeneration And Transport. *Nature Methods*, 2005, vol. 2, no. 8, pp. 599-605. ISSN 1548-7105.

[63] FORRÓ, C. et al. Modular microstructure design to build neuronal networks of defined functional connectivity. *Biosensors and Bioelectronics*, 2018, vol. 122, pp. 75.87. ISSN 0956-5663.

[64] JAMES, C. D. et al. Aligned Microcontact Printing Of Micrometer-Scale Poly-L-Lysine Structures For Controlled Growth Of Cultured Neurons On Planar Microelectrode Arrays. *IEEE Transactions on Biomedical Engineering*, 2000, vol. 47, no. 1, ISSN 1558-2531.

[65] NAM, Y., BRANCH D. W. and WHEELER, B. C. Epoxy-silane linking of biomolecules is simple and effective for patterning neuronal cultures. *Biosensors and Bioelectronics*, 2006, vol. 22, no. 5. pp. 589-597. ISSN 0956-5663.

[66] JUN, S. B. et al. Low-density neuronal networks cultured using patterned poly-l-lysine on microelectrode arrays. *Journal of Neuroscience Methods*, 2007, vol. 160, no. 2, pp. 317-326. ISSN 0165-0270.

[67] JUNGBLUT, M. et al. Triangular Neuronal Networks On Microelectrode Arrays: An Approach To Improve The Properties Of Low-Density Networks For Extracellular Recording. *Biomedical Microdevices*, 2009, vol. 11, no. 6. pp. 1269-1278. ISSN 1572-8781.

[68] MARCONI, E. Emergent Functional Properties Of Neuronal Networks With Controlled Topology. *PLoS One*, 2012, vol. 7, no. 4. ISSN 1932-6203.

[69] BANERJEE, I., PANGULE, R. C. and KANE R. S. Antifouling Coatings: Recent Developments In The Design Of Surfaces That Prevent Fouling By Proteins, Bacteria, And Marine Organisms. *Advanced Materials*, 2011, vol. 23, no. 6. ISSN 1521-4095.

[70] THÉRY, M. and PIEL M. Adhesive micropatterns for cells: a microcontact printing protocol. *Cold Spring Harbor Protocols*, 2009, no 7. ISSN 15596095.

[71] KIM, J. M., IM, C. and LEE, W. R. Plateau-Shaped Flexible Polymer Microelectrode Array For Neural Recording. *Polymers (Basel)*, 2017, vol. 9, no. 12. ISSN 2073-4360.

[72] MATTOX, D. *Interface Formation and the adhesion of deposited thin films*. New Mexico, USA: Technical Information Division Sandia Corporation Albuquerque, 1965. In Monograph, R65852.

[73] JOHNSTON, I. D. et al. Mechanical characterization of bulk Sylgard 184 for microfluidics and microengineering. *Journal of Micromechanics and Microengineering*, 2014, vol. 24. ISSN 1361-6439.

[74] XIA, Y. and WHITESIDES, G. M., Soft Lithography. *Annual Review of Materials Research*, 1998, vol. 28, pp. 153-184. ISSN 1545-4118.

[75] QIN, D., XIA, Y. and WHITESIDES, G. M. Soft lithography for micro- and nanoscale patterning. *Nature Protocols*, 2010, vol. 5, no. 3, pp. 491-502. ISSN 1750-2799.

[76] ELBERT, D. L. and HUBBELL, J. A. Self-Assembly And Steric Stabilization At Heterogeneous, Biological Surfaces Using Adsorbing Block Copolymers. *Chemistry & Biology*, 1998, vol. 5, no. 3, pp. 177-183. ISSN 1074-5521.

[77] TU, X. et al. Patterned Parylene C For Cell Adhesion, Spreading And Alignment Studies. *Microelectronic Engineering*, 2017, vol. 175, no. C. ISSN 0167-9317.

[78] CHANG, T. Y. et al. Cell And Protein Compatibility Of Parylene-C Surfaces. *Langmuir*, 2007, vol. 23, no. 23, pp. 11718-11725. ISSN 1520-5827.

Author's publications

Papers:

SLAVÍK, J.; SKOPALÍK, J.; PROVAZNÍK, I.; HUBÁLEK, J. Multi-Electrode Array with a Planar Surface for Cell Patterning by Microprinting. *Sensors*, 2019, vol. 19, no. 24, p. 1-11. ISSN: 1424-8220

SLAVÍK, J.; TRNKOVÁ, L.; HUBÁLEK, J. Interaction of selenite with metallothionein studied by Brdička reaction. Monatshefte für Chemie, 2019, vol. 150, no. 3, p. 469-475. ISSN: 0026-9247

YAN, J.C.; CHEN, Y.; PANG, Y.; SLAVÍK, J.; ZHAO Y.F.; WU, X.M.; YANG, Y.; YANG, S.F.; REN, T.L. A Miniaturized Colorimeter with a Novel Design and High Precision for Photometric Detection. *Sensors*, 2018, vol. 18. no. 3, p. 1-14. ISSN: 1424-8220

Submitted papers:

SLAVÍK, J.; ČMIEL, V.; HUBÁLEK, J.; YANG, Y.; REN, T.L. et al. Hippocampal neurons patterning on quartz grooves and parylene cues on quartz substrate. Applied Sciences. ISSN 2076-3417. (Submitted publication)

Conference – abstract:

SKOPALÍK, J.; SLAVÍK, J.; ČMIEL, V.; POLÁKOVÁ, K.; PRŮCHA, J.; GABRIELOVÁ, E.; BAIAZITOVA, L.; SVOBODA, O.; PROVAZNÍK, I. *Comparison of PDMS Microtopographical Plates and Planar Nanofiber Scaffolds for In Vitro Cultivation of Cardiac Cells.* Nanocon 2018 - Abstracts. 1. Brno, Czech Republic: 2018. p. 109-109. ISBN: 978-80-87294-85-7.

Conference – abstract and oral presentation:

TRNKOVÁ, L.; SLAVÍK, J.; HUBÁLEK, J. *Metallothionein and selenite in Brdička reaction*. . XIX. Workshop of Biophysical Chemists and Electrochemists. *Book of abstracts. Brno: Masaryk University Press, 2019, p. 57-58. ISBN 978-80-210-9309-6.*

Conference – abstract and poster:

SLAVÍK, J.; HUBÁLEK; J. *Microfluidic chip with amperometric detection for monosacharides determination*. *XV. Workshop of Physical Chemists and electrochemists. Book of abstracts. Brno: Masaryk University Press, 2015. p. 161-164. ISBN: 978-80-210-7857-4.*

Internship:

Doctoral internship (1.9.2015-31.8.2017); Institute of Microelectronics, Tsinghua University, Beijing 100084, China